Acta Astronautica 175 (2020) 540–569

Contents lists available at ScienceDirect

Acta Astronautica

journal homepage: www.elsevier.com/locate/actaastro

A review towards the design of extraterrestrial structures: From regolith to human outposts

Nicos Kalapodis[a,*], Georgios Kampas[a], Olga-Joan Ktenidou[b]

[a] School of Engineering, University of Greenwich, Central Avenue, ME4 4TB, Chatham, United Kingdom
[b] Institute of Geodynamics, National Observatory of Athens, 11810, Athens, Greece

ARTICLE INFO

Keywords:
Extraterrestrial structures
Regolith
Inflatable structures
Additive manufacturing
Strong ground motions

ABSTRACT

The design of a permanent human habitat on a planetary body other than the Earth is an idea introduced many decades ago, which became even more significant after the landing of the first humans on the Moon with the Apollo missions. Today's rampant technological advances combined with ambitious missions, such as the Insight mission on Mars and the Artemis program for the Moon, render the vision of space colonization more realistic than ever, as it constantly gains momentum. There is a considerable number of publications across several disciplines pertaining to the exploration of Lunar and Martian environments, to those planets' soil properties, and to the design of the first habitable modules. The scope of this paper is to present a meticulous selection of the most significant publications within the scientific areas related to: (a) geotechnical engineering aspects, including the mechanical properties and chemical composition of Lunar and Martian regolith samples and simulants, along with elements of anchoring and rigid pads as potential forms of foundation; (b) ground motions generated by different types of Moonquakes and meteoroid impacts; (c) the different concepts and types of extraterrestrial (ET) structures (generic, inflatable, deployable, 3D-printed), as well as overall views of proposed ET habitats. Apart from the details given in the main text of this paper, a targeted effort was made to summarize and compile most of this information in representative tables and present it in chronological order, so as to showcase the evolution of human thinking as regards ET structures.

1. Introduction

The concept of creating extraterrestrial habitats predates what is known as the “space age”, which started in 1957 with the first Apollo Lunar landing. Nowadays, following the space boom originated by both federal bodies (NASA, ESA, ISRO, etc.) and private firms (SpaceX, Blue Origin, Virgin Galactic, etc.), it has become evident that there will soon be a need to expand civil engineering towards the design and construction of Lunar and Martian structures, habitats and outposts [1,2].

The first step towards the “urban development” on other planetary bodies is for both scientists and engineers to fully comprehend the extraterrestrial environmental conditions. To this end, Jablonski and Showalter [3]; Benaroya [4] and Schrunk et al. [5], review the current data about the Lunar environmental conditions (e.g. low gravity, temperature fluctuation, radiation, lack of atmosphere and pressure, meteoroid impacts, Lunar dust, and other geophysical features) and highlight the most significant requirements for Lunar systems and structures that can be important especially in the earlier stages of Lunar explorations. In particular, the long duration of the Lunar day (29.53 Earth days) along with the almost non-existent Lunar atmosphere result in high temperature fluctuations (up to 280 K or °C) on the Moon's surface, where any prospective Lunar structure is bound to be constructed [6,7]. Furthermore, the extremely hazardous radiation that is caused by either galactic cosmic rays (GCR) or solar energetic particles (SEO) [8] will pose a great threat to the subsystems of any Lunar structure (e.g., a deployable system) [9]. The lack of atmosphere renders the Moon vulnerable to meteoroid impacts: impactors with velocities that vary from 2.4 km/s to 72 km/s [4] and weighing from less than 1 kg to over 5 tons in rarer cases [10] can be expected to severely affect Lunar structures in the vicinity of where they land. Additionally, Lunar dust as a material can prove quite dangerous and should be taken into consideration [4,7]. The Lunar gravitational acceleration at ground surface level is approximately $1.62\frac{m}{s^2}$ or (0.17**g**), where g= $9.81\frac{m}{s^2}$ on Earth [11]; amongst others). Hence, since gravity plays a less significant role, some of the prospective structures will be able to span longer without a problem [4]. Moreover, the authors in their recent work [12,13] have highlighted the effect of microgravity on the dynamic properties and performance of fundamental structural dynamic

* Corresponding author.
E-mail address: n.kalapodis@greenwich.ac.uk (N. Kalapodis).

https://doi.org/10.1016/j.actaastro.2020.05.038
Received 17 March 2020; Received in revised form 10 May 2020; Accepted 19 May 2020
Available online 26 May 2020

systems.

In recent years, research has been conducted towards new technologies for the development and construction of habitats on the surface of Mars as well, by considering different architectural concepts combined with basic and, in most cases, simplistic structural analysis. The challenges on Mars (e.g., low gravity, atmospheric conditions, lack of water, radiation levels, etc.) from a civil engineering perspective are discussed by Petrov and Oschendorf [14] and Schock and Caleb Hing [15]; where recommendations are given for the design of a Martian colony. More specifically, the mean surface gravity on Mars is approximately equal to $3.71\frac{m}{s^2}$ or $(0.38\mathbf{g})$ [16]. Regarding the atmosphere's characteristics, the total atmospheric pressure averages about 6 mbar, which corresponds to 0.6% of the Earth's atmospheric pressure [17]. The temperature fluctuation depends on many parameters (geographic location, observation techniques, etc.), which are described in detail by Jakosky & Phillips [17]; Gurwell et al. [18] and Wilson [19].

The present paper aims to serve as a stepping stone for expanding civil engineering towards the design and construction of extraterrestrial structures (in both a Lunar and Martian environment), considering and reviewing the most significant pertinent literature. More specifically, the objective is to cover a wide spectrum of fields and aspects, starting from the mechanical properties of the surface material (Lunar and Martian regolith) and from the identification of ground motion-related hazards (extraterrestrial seismology, covering both indigenous seismicity and impacts from foreign bodies), to potential foundation systems (anchoring and landing pads) and most importantly to the architectural and structural design proposals for Lunar and Martian modules and outposts (generic, inflatable, deployable and 3D-printed structures). It is our belief that bringing together elements from these very different disciplines will strengthen and benefit the truly multidisciplinary community of scientists and engineers working towards space exploration and facilitate progress in ET construction.

2. Aspects of geotechnical engineering

This section covers a wide range of geotechnical engineering aspects that constitute the basis for further civil engineering analysis. The first paragraphs pertain to the investigation of Lunar and Martian regolith mechanical and chemical properties. Subsequently, the section presents additional information regarding anchoring within regolith layers and developing landing pads using regolith, which could be potentially used as primitive forms of foundations.

Regolith has been defined as a general term to describe the layer of fragmented and unconsolidated rock materials, whose way of their forming varies from one place or planetary body to another. In particular, regolith is produced on Earth through uniquely terrestrial processes exploiting the presence of oxygen, the influence of wind and water, and other earthly activities (e.g. Refs. [20]. On the other hand, the Lunar regolith resulted from the continuous impact of meteoroids and the bombardment of the Lunar surface by charged particles mainly from the Sun [21]. The Martian regolith is a mix of weathered and windblown material. The upper-5-m layer of Martian regolith is mainly composed of almost cohesionless basaltic sand and a few rocks. Regarding the deeper layers, it is expected that they consist of a plethora of larger particles and rocks [22]. This section incorporates results from a large number of past studies that have examined the mechanical properties of both Lunar and Martian regolith, be it on the original materials and artificial simulants. The importance of this section is clearly associated with any ET geotechnical engineering design and works that may need to be conducted (excavations, landing pads, etc).

2.1. Lunar regolith

2.1.1. Original samples tested on Earth

A thorough review of the physical and mechanical properties of the original Lunar regolith acquired through direct investigations of the Lunar surface by manned and automated missions is presented by Slyuta [23]. In particular, the main mechanical and physical properties of the Lunar soil –such as density, porosity, granulometric composition, adhesion, apparent cohesion, deformation characteristics (modulus of elasticity and Poisson ratio), angle of internal friction, shear and compressive strength and bearing capacity in conjunction with the ground depth– are considered by Leonovich et al. [24]; Leonovich et al. [25] and Slyuta [23]; among others. From the scope of civil engineering, the relative density Dr (%), apparent cohesion (c') and internal friction angle (ϕ') are of crucial importance. The internal friction angle is expressed by the formula:

$$\phi' = \arctan\left(\frac{\tau - c'}{\sigma'}\right) \tag{1}$$

where c' is the apparent cohesion, σ' is the effective normal stress and τ is the shear stress expressed in kPa. These three parameters combined represent the Mohr-Coulomb envelope. Furthermore, the relative density is determined by the following expression [26]:

$$D_R = \frac{\rho_{max}}{\rho} \cdot \frac{\rho - \rho_{min}}{\rho_{max} - \rho_{min}} \cdot 100\% \tag{2}$$

where ρ is the bulk density of Lunar regolith, and ρ_{min} and ρ_{max} are the minimum and maximum values of the Lunar regolith's bulk density. It has been observed that D_R increases abruptly between the depths of 10 and 20 cm [27]. Furthermore, Houston et al. [27] related the bulk density and relative density (D_R) with the corresponding layer thickness of the Lunar surface samples obtained by the Apollo 15 through 17 missions. These results are shown in Table 1. The sharp change in the regolith's D_R at the surface layer combined with the very high values of D_R of the regolith soil at larger depths, stems from the fact that the Lunar surface is constantly bombarded by meteoroids that loosen the surface layers and compact the lower ones [26]. Such observations can be very important, since they affect both the landing process and any required excavations in microgravity conditions. Furthermore, the aforementioned density distribution has a strong effect on the distribution with depth of the regolith's shear strength.

The loose state of the surface Lunar soil is characterized by insignificant apparent cohesion (c') and very small values of internal friction (ϕ'). On the other hand, as illustrated in Fig. 1, when the depth increases, the compactness of the soil and the cohesion as well and eventually, for bulk density values over $1.5g/cm^3$, the angle of internal friction approaches 25^o [25]. Table 2 presents the values of the apparent cohesion (c') and angle of internal friction (ϕ') pertaining to original Lunar regolith samples, collected by various missions [23,37]. The missions that investigated soil parameters to date are the following: Lunar Orbiter (1966), Surveyor I (1966), Surveyor III (1967), Surveyor VI (1967), Apollo 11 (1969), Apollo 12 (1969), Apollo 14 (1971), Apollo 15 (1971), Apollo 16 (1972), and Luna 16 (1970). The techniques that yielded these results vary significantly, ranging from standard in-situ tests such as penetrometer, to innovative in-situ techniques such as studying the tracks left by the small vehicle and compare them to those left in the lab on Earth, [21,32].

The depth of the Lunar soil plays an important role since it affects the values of the apparent cohesion and internal friction. With the aid of various techniques, the mean value of the apparent cohesion and the friction angle were measured down to 60 cm of the Lunar surface at

Table 1
Lunar soil density according to depth range [27].

Depth range (cm)	Bulk density, ρ ($\mathbf{g/cm^3}$)	Relative density, $\boldsymbol{D_R}$ (%)
0–15	1.50 ± 0.05	65 ± 3
0–30	1.58 ± 0.05	74 ± 3
30–60	1.74 ± 0.05	92 ± 3
0–60	1.66 ± 0.05	83 ± 3

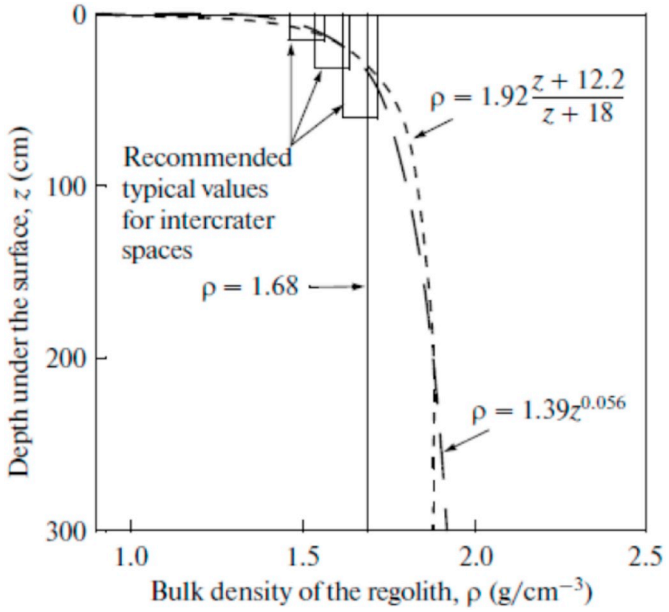

Fig. 1. The hyperbolic dependence of the bulk density of Lunar regolith versus depth (dashed curve) [28].

plains between the craters and were found to be equal to 1.6 kPa and 49° respectively [28]. The exact distribution of the typical values of the apparent cohesion and friction angles is presented on Table 3 [28]. More specifically, during the Apollo 11 and 12 missions, estimation of the Lunar soil's shear strength was crudely made by means of physical interaction with the Lunar surface (e.g., by observing the Lunar Module landing, the astronaut's footprints or by the penetration of the flag's pole into the soil). More accurate techniques were used during the Apollo 14 mission, where the experiments for the evaluation of the shear strength were conducted a) by excavating a shallow trench at the surface and b) by pushing the Apollo Simple Penetrometer (ASP) –which was a simple rod-into the surface. A more sophisticated Self-Recording Penetrometer (SRP) was operated by the astronauts on the Apollo 15 and 16 missions. Furthermore, cone penetrometer tests were vastly used in all Lunar missions except for Apollo 11–12.

2.1.2. Lunar simulants

Before the Apollo 11 mission in 1969, when 13 kg of original Lunar soil samples were brought back to Earth, no regolith simulant was available for engineering studies. By the end of 1972, a total amount of 115 kg Lunar regolith had been brought to Earth by the Apollo missions and also, between 1970 and 1976, an amount of 321 gr Lunar regolith had been brought to Earth by the Luna missions [38–40]. Nevertheless, the original Lunar samples collected were not sufficient for engineering studies. Since 1970, i.e. for the past five decades, no further material has been collected. Therefore, the production of Lunar regolith

Table 3
Typical values of cohesion and internal friction angle for a Lunar surface ground layer of 60 cm [28]. The mean and range of values are given.

Depth interval (cm)	Cohesion (kPa)		Internal friction angle (°)	
	mean	range	mean	range
0–15	0.52	0.44–0.62	42	41–43
0–30	0.90	0.74–1.10	46	44–47
30–60	3.00	2.40–3.80	54	52–55
0–60	1.60	1.30–1.90	49	48–51

simulants is of high importance. Lunar regolith simulants are terrestrial materials composed chemically in such a way as to approximate the physical, mechanical, or engineering properties of the original regolith samples. In practice, it is not feasible to produce a simulant with the same physical and mechanical properties and chemical composition as the original Lunar regolith. Thus, each Lunar regolith simulant is developed in order to simulate one or two target properties of the real sample, depending on the use. For example, rocks of a basaltic composition are able to simulate mare Lunar soil (large dark lava-filled basaltic basins on the Lunar surface, formed by volcanic activity), while Lunar highland soils (mountainous regions on the Lunar surface, where the rocks are largely Anorthosites, a kind of igneous rock that forms when lava cools more slowly than in the case of basalts) can be better simulated by earthen anorthosites admixed with pyroxene and olivine [24]. Attempts to quantify the mechanical properties of regolith simulants have been made since the 1990s and have continued to date. Table 4 summarizes the best-known simulants along with a brief description and associated mechanical properties, including relative density, cohesion and angle of friction.

Since the mechanical characteristics of the original Lunar samples are related to their chemical composition, the most significant oxides for both the original samples and the simulants are presented as mass fractions (wt%) in Table 5. By observing Table 5, one may conclude that Silicon dioxide (SiO_2), Aluminum oxide (Al_2O_3), Iron oxide (FeO) and Calcium oxide (CaO) are the most prevalent constituents of the Lunar soil.

2.2. Martian regolith

2.2.1. Original material tested in-situ

A plethora of studies have been carried out on the physical and mechanical properties of surface Martian regolith. These properties have been provided by the interaction of arm scoops and rover wheels used by the successful landers (Viking Landers 1 and 2, Phoenix lander) and rovers (Sojourner rover of Mars Pathfinder—MPF, Spirit and Opportunity rovers of Mars Exploration Rovers— MERs, and Curiosity—Mars Science Laboratory) respectively [58]. In particular, the two Viking landers and the Phoenix lander were equipped with mechanical sampler arms able to trench the Martian surface. Motor currents from the arms were recorded during the sample collection, to

Table 2
Geotechnical properties of the original Lunar regolith samples.

Mission	Description	Cohesion (kPa)	Internal friction angle (°)	Reference
Lunar Orbiter (1966)	Boulder track analysis	0.35	33	Nordmeyer (1967) [29]
Surveyor I (1966)	Strain gage and TV data	0.15–15	55	Jaffe (1967) [30]
Surveyor III and VI (1967)	Soil mechanics surface sampler	0.35–0.70	35–37	Scott and Roberson (1969) [31]
Lunar Orbiter (1966)	Boulder track analysis	0.1	10–30	Moore (1970) [32]
Apollo 11 (1969)	Penetrometer tests in LRL on bulk soil sample	0.3–1.4	35–45	Costes et al. (1970) [33]
Apollo 11 (1969)	Penetration of core tubes, flagpole, SWC shaft	0.8–2.1	37–45	Costes et al. (1971) [34]
Apollo 12 (1969)	Penetration of core tubes, flagpole, SWC shaft	0.6–0.8	38–44	Costes et al. (1971) [34]
Apollo 14 (1971)	Soil mechanics trench	<0.03–0.3	35–45	Mitchell et al. (1971) [35]
Apollo 15 (1971)	Measured at station 8	1.92–2.01 (typical 1.97)	47.5–51.5 (typical 49.5)	Mitchell et al. (1972b) [36]
Luna-16 (1970)	Lunar soil from Mare Fecunditatis	5.1	25	Leonovich et al. (1974) [25]

Table 4
Mechanical properties of Lunar regolith simulants.

Simulant	Description	ρ (g/cm^3)	D_R (%)	c' (kPa)	φ' (°)	Reference
JSC-1	The simulant was created at the Johnson Space Center (JSC), USA, targeting Lunar mare regolith. It contains a low percentage of titanium and a high abundance of glass.	1.90	–	0.2	49	Perkins et al. (1991) [41]
		–	–	2.4–3.8	52–55	Carrier et al. (1991) [28]
		1.50 1.60 1.65	–	≤1	45	McKay (1994) [42,43]
		1.62 1.72	40 60	3.9 13.4	44.4 52.7	Klosky et al. (1996) [44]
		1.33–1.80	–	0	48–64	Perkins and Madson (1996) [45]
		1.62 1.72 1.81	–	3.9 6.2 14.4	44.3 49.5 53.6	Klosky et al. (2000) [46]
FJS-1	This simulant originated in Japan (Fuji volcano) and was designed to simulate the low-titanium Lunar soil brought by the Apollo 14 mission	1.55	–	8	37.2	Kanamori et al. (1998) [47]
FJS-2	It contains more olivine and simulates the properties of the Apollo 14 soil better than FJS-1	1.55	–	3	39.4	
FJS-3	It was produced by adding ilmenite and olivine in FJS-1 and can simulate the properties of the Apollo 11 soil	1.55	–	4	32.5	
MLS-1	This simulant was developed in the University of Minnesota, USA, and can simulate the properties of the Apollo 11 sample	1.56–2.20	–	0	48–58	Perkins and Madson (1996) [45]
JSC-1A	JSC-1A is a modification of JSC-1, targeting the mare Lunar regolith. It is mined in the volcanic field of the San Francisco area.	–	53–95	3.9–14.4	44.4–53.6	Klosky et al. (2000) [46]
		1.63–1.88	20–75	2.0–5.0	37–48	Alshibli and Hasan (2009) [48]
		1.66–1.94	24.6–84.6	–	41.87–56.70	Zeng et al. (2010) [49]
TJ-1	The simulants are created with the use of volcanic ash deposits collected from northern China. These are simulants of low-titanium basaltic regolith produced by Tongji University in China.	1.36	–	0.86	47.6	Jiang et al. (2012) [50]
TJ-2		1.45	–	1.03	46.9	Jiang et al. (2012) [50]
GRC-3	This simulant was created using Bonnie silt (which is a natural loess) excavated from a site in Burlington, Colorado (US). Such a simulant is applied for the evaluation of traction forces to the wheels of a rover.	1.63–1.84	30.4–80.3	–	37.8–47.8	He et al. (2013) [51]
CAS-1	This simulant is composed of low-titanium basaltic scoria from the Changbai mountains in northeast China and was developed by the Chinese Academy of Science to support the Lunar orbiter mission. It is designed to match the Lunar sample brought by the Apollo 14 mission.	1.03–2.04 (Compacted-state density) 0.73–1.72 (Loose-state density)	–	0–12	33.3–41.8	Lu and Jianguo (2014) [52]
BP-1	It is developed by the Kennedy Center/Arizona, USA, and consists of crumbled basalt. It also matches the low-titanium Lunar soil of basaltic composition.	1.43–1.86	–	0–2.0	39–51	Suescun-Florez et al. (2015) [53]

provide additional data on surface material properties [59–62]. Furthermore, the two Mars exploration rovers (Spirit and Opportunity), the Mars Science Laboratory rover (Curiosity) and the Mars Pathfinder rover (Sojourner), carried out wheel trenching and terramechanic experiments during which they were monitoring the motor currents in order to obtain wheel torques and pictured the deformed materials [63–66]. Such experiments led to the evaluation of the basic physical and mechanical characteristics of Martian soil, such as the apparent cohesion, the bulk density and the angle of internal friction [64,67]; and [68]. The aforementioned characteristics are presented in Table 6.

The most recent space expedition is the InSight mission, which constitutes the first geophysics-oriented mission to another planet. Through this mission, two instruments (the SEIS seismometer and the HP3 heat flow probe) interact directly with the regolith on the surface of Mars in order to evaluate the structure of Mars [71]. InSight is the product of many years of engineering, scientific design and preparations. More specifically, the InSight lander is based on the lander which was used in the Phoenix mission and was launched to Mars in August 2007 for the observation of near-surface ice in the Martian Arctic [72]. The Heat Flow and Physical Properties Package (HP3) of InSight includes a mole that was designed to hammer itself into the regolith with a target depth of 5 m [73]. This was meant to also help constrain soil

Table 5
Chemical composition of the Lunar original samples and their simulants.

Oxide (wt%)	Original Lunar Samples (Mean values)									Lunar Simulants (Mean values or ranges)								
	Apollo Missions						Luna Missions			Made in US				Made in Japan			Made in China	
	11	12	14	15	16	17	16	20	24	MLS-1	JSC-1	JSC-1A	BP-1	FJS-1	FJS-2	FJS-3	TJ-1	CAS-1
	(a)	(a)	(a)	(a)	(a)	(a)	(a)	(a)	(a)	(b)	(c)-(d)	m.d*	(e)	(a)	(a)	(a)	(f)	(g)
SiO2	42.2	46.3	48.1	46.9	45	43.2	41.7	45.1	43.9	43.9	47.7	46–49	47.2	49.1	49.7	46	47.7	49.24
TiO2	7.8	3	1.7	1.4	0.54	4.2	3.4	0.55	1.3	6.3	1.6	1–2	2.3	1.9	1.7	6.7	2	1.91
Al2O3	13.6	12.9	17.4	14.6	27.3	17.1	15.3	22.3	12.5	13.7	15	14.5–15.5	16.7	16.2	14.8	13.7	16.2	15.8
Cr2O3	0.3	0.34	0.23	0.36	0.33	0.33	0.28	–	0.32	–	0.04	0.02–0.06	–	–	–	–	–	–
FeO	15.3	15.1	10.4	14.3	5.1	12.2	16.7	7	19.8	13.4	7.4	7–7.5	6.2	8.3	8.2	7.9	–	11.47
Fe2O3	–	–	–	–	–	–	–	–	–	2.6	3.4	3–4	5.9	4.8	4.7	5.9	10.75	–
MnO	0.2	0.22	0.14	0.19	0.3	0.17	0.23	0.13	0.25	0.2	0.18	0.15–0.20	0.21	0.19	0.19	0.28	0.15	0.14
MgO	7.8	9.3	9.4	11.5	5.7	10.4	8.8	9.8	9.4	6.7	9	8.5–9.5	6.5	3.8	8.1	7.3	5.04	8.72
CaO	11.9	10.7	10.7	10.8	15.7	11.8	12.5	15.1	12.3	10.1	10.4	10–11	9.2	9.1	8.4	7.8	8.21	7.25
Na2O	0.47	0.54	0.7	0.39	0.46	0.4	0.34	0.5	0.31	2.1	2.7	2.5–3	3.5	2.8	2.6	2.6	4.92	3.08
K2O	0.16	0.31	0.55	0.21	0.17	0.13	0.1	0.1	0.04	0.28	0.82	0.75–0.85	1.1	1	0.92	0.87	2.29	1.03
P2O5	0.05	0.4	0.51	0.18	0.11	0.12	0.12	0.16	0.11	0.2	0.66	0.6–0.7	0.52	0.44	0.4	0.39	0.58	0.3
BaO	–	–	–	–	–	–	–	–	–	–	–	–	–	–	–	–	0.06	–
NiO	–	–	–	–	–	–	–	–	–	–	–	–	–	–	–	–	–	–
SrO	–	–	–	–	–	–	–	–	–	–	–	–	–	–	–	–	0.09	–
S	0.12	–	–	0.06	0.07	0.09	0.21	0.08	0.14	–	–	–	–	–	–	–	–	–
H2O	–	–	–	–	–	–	–	–	–	–	–	–	–	0.43	0.47	0.58	–	–
Total	99.9	99.6	99.8	100.8	100.8	100.5	99.7	100.8	100.4	99.5	98.9		99.33	98.14	100.2	100	98.9	99.46

*m.d.: Manufacturer Data (a) Kanamori et al. (1998) [47] (b) Weiblen et al. (1990) [54] (c) McKay et al. (1993) [55] (d) McKay et al. (1994) [42,43] (e) Jiang et al. (2012) [50] (f) Zheng et al. (2009) [56] (g) Stoeser and Rickman (2010) [57].

Table 6
Mechanical properties of the surface Martian regolith.

Mission	Description	ρ (g/cm^3)	c'(kPa)	ϕ'(deg)	Reference
Viking Lander 1	Scoop trenching and landing pad sinking	1.15 ± 0.15	1.6 ± 1.2 0–3.7	18 ± 2.4	Moore et al. (1982) [69] Moore et al. (1987) [70] Moore & Jakosky (1989) [67]
Viking Lander 1	Scoop trenching and landing pad sinking	1.60 ± 0.40	5.1 ± 2.7 2.2–10.6	30.8 ± 2.4	Moore et al. (1982) [69] Moore et al. (1987) [70] Moore & Jakosky (1989) [67]
Viking Lander 1 & 2	Scoop trenching and landing pad sinking	2.60	1–10	40–60	Moore et al. (1982) [69] Moore et al. (1987) [70] Moore & Jakosky (1989) [67]
Viking Lander 2	Scoop trenching and landing pad sinking	1.40 ± 0.20	1.1 ± 0.8 0–3.2	34.5 ± 4.7	Moore et al. (1982) [69] Moore et al. (1987) [70] Moore & Jakosky (1989) [67]
MPF Sojourner	Wheel dig trenching	2.0–2.2	0.34–0.57	31.4–42.2	Moore et al. (1999) [63]
MPF Sojourner	Wheel dig trenching	1.07–1.27	0.18–0.53	15.1–33.1	Moore et al. (1999) [63]

mechanical parameters such as bulk density, cohesion, and friction angle [68]. Currently (May 2020), the mole is progressing very slowly, likely due to the high strength (namely cohesion) of a near-surface layer of cemented sand called the duricrust [74]. Thus, the new estimates of mechanical martian regolith properties are still pending. However, based on slope stability back-analyses from the pits formed under the lander, a minimum cohesion of 1–2 kPa is estimated [75].

2.2.2. Martian simulants

In the case of Mars, the need for simulants is even more evident than in the Lunar case, because martian regolith was only tested in-situ and samples were never brought back to Earth for laboratory testing. Aiming to support the space missions, various tests incorporating rovers and their equipment and laboratory experiments have included different Martian regolith simulants [76]. Table 7 compiles the mechanical characteristics of the most common Martian soil simulants along with a short description.

Similarly to section 2.1 on Lunar simulants, the most significant constituents of the Martian soil are compiled in Table 8, where it is apparent that the Lunar and Martian regolith soil composition have common characteristics. More specifically, oxides like Silicon dioxide (SiO_2) and Aluminum oxide (Al_2O_3) are the most abundant components for both Martian and Lunar soil, being almost of the same weight percentage.

2.3. Summary of the mechanical characteristics of Lunar and Martian original material and simulants

To our knowledge, a detailed compilation and comparison of all known experiments yielding Lunar/Martian material mechanical properties (be it on samples or simulants) does not exist to date. We feel that such a compilation is well worth producing and that it will serve as a reference for future studies not only of material properties but also –and more notably-for the study of any geotechnical issues pertaining to ET construction. The nature of the samples/simulants in itself (e.g., different extraction locations/years, different construction methods/materials) implies a significant degree of variability in the properties estimated. We believe it is important to map the uncertainties and variabilities attached to the cohesion and friction angle across all existing experiments to date. This will allow future studies to easily

Table 7
Mechanical properties of Martian regolith simulants.

Simulant	Description	ρ (g/cm3)	D_R (%)	c' (kPa)	φ' (deg)	Reference
JSC Mars-1	Accounts for the oxidized Martian soil and is a fraction of altered volcanic ash from a cindered one that originates in Hawaii	0.835	0–96	1.91	47	Allen et al. (1998) [77]
		0.90–1.15		0.61–0.85	40.8–41.4	Perko et al. (2006) [76]
JPL Lab 107	Collected at the Jet Propulsion Laboratory (JPL); consists of dust-free washed silica sand	1.47–1.67	26–100	0.67–1.41	33.3–33.7	Perko et al. (2006) [76]
JPL Lab 82	Collected at JPL; consists of dust-free washed ruby garnet mix	2.44–2.56	64–95	0.69–0.99	33.7–38.3	Perko et al. (2006) [76]
MER Yard 317	Obtained from the indoor MER test facility and created by crushing volcanic rock	1.48–1.69	14–74	1.49	47.9–53.3	Perko et al. (2006) [76]
MARS Yard	Taken from the outdoor Mars Yard and created by decomposed granite brick cinder and dust from washed sand	1.62–1.79	45–103	0.93–0.99	35.1–37.2	Perko et al. (2006) [76]
MMS sand I	Basaltic simulant in rock, sand and dust form. The source rock of the simulant is mined from the Tertiary Tropico group in the western Mojave	1.384		0.81	38	Peters et al. (2008) [78]
MMS sand II	desert. The sand and dust gradients are produced by mechanically crushing basaltic boulders.	1.341		1.96	39	Peters et al. (2008) [78]
MMS dust I		1.078		0.38	31	Peters et al. (2008) [78]
MMS dust II		0.911		0.53	30	Peters et al. (2008) [78]
ES-1	Sandy material, based upon Nepheline sternoy 7. Intended to resemble the characteristics of the top-soil on Mars.	1.30		0.50–1.50	16–21	Brunskill et al. (2011) [79]
		1.50		0.50–2.00	18–24	
ES-2	Sandy material, based upon Red Hill 110. Intended to resemble the characteristics of the terrestrial medium-fine to coarse quartz sands.	1.45		0.00–1.50	23–27	Brunskill et al. (2011) [79]
		1.60		0.00–1.50	29–34	
ES-3	Sandy material, based upon Leighton buzzard DA 30. Intended to resemble the characteristics of the terrestrial medium-fine to coarse quartz sands.	1.55		0.00–0.30	30–40	Brunskill et al. (2011)
		1.80		0.00–0.30	35–42	
JMSS-1	Developed by the Chinese Academy of Science. Produced by the mechanical crushing of Jining basalt including small amounts of magnetite and hematite.	1.45		0.33	40.6	Zeng et al. (2015)

account for their sensitivity, and avoid introducing bias by selecting e.g. values based on a small part of the available literature. To this end, the mechanical characteristics (cohesion and angle of shearing resistance) of the original Lunar and Martian regolith along with the corresponding simulants previously presented in sections 2.1 and 2.2 are summarized in Fig. 2. Fig. 2 is complemented by Table 9, where all the original samples and simulants are numbered.

2.4. Anchoring in regolith

One of the challenges with prospective structures in extraterrestrial environments is the consideration of any type of foundation. The microgravity conditions along with the uncertainties of the Martian and Lunar regolith as a material forced researchers to focus on drilling methods, aiming to evaluate the efficiency of anchoring as a foundation method. Therefore, anchoring can be envisaged as a basic foundation method for modular extraterrestrial structures in microgravity environments in order to avoid deep excavations and prevent potential uplifting. It can also guarantee the stability of landers and it also constitutes a very useful tool for rovers, which can set an anchor before entering into a dangerous zone, with a view to winch themselves out in an urgent situation [87]. Errourney and Benaroya [88] have investigated the static and dynamic behavior of regolith during drilling and anchoring, as a potential foundation system. Various researchers who have proposed different drilling techniques for anchoring in extraterrestrial environments are summarized in Table 10 and its accompanying Fig. 3.

2.5. Regolith-based landing pads

As mentioned above, foundations that demand extensive excavations most likely would not be preferred as a practical solution for extraterrestrial environments, given the inherent uncertainties. Furthermore, there is no evident reason for a vertical urbanization on the Moon or Mars that could lead to “heavier” structures and thus deeper foundations. Hence, the interest shifts towards free-standing structures. To this end, the design and construction of pads utilizing local regolith is essential; their key advantage is their versatility and reusability: besides their use as landing pads for rockets, they can be then used as rigid foundation rafts for structures.

Regarding their use for rocket landing, pads can mitigate dust problems and plume effects during the rocket's touchdown and takeoff. Furthermore, Metzger et al. [92] highlight that the exhaust plume ejected by the engines of a future manned spaceflight will create large holes/craters in the ground surface as shown in Fig. 4, and can cause damage to the lander's base due to rock impacts. Additionally, it can cause instability and tilting phenomena to the craft due to land subsidence stemming from the aforementioned residual crater.

Aiming to resolve the above issues on the Lunar surface, Lee et al. [93] present a construction technique based on the in-situ resources utilization (ISRU) framework. Owing to its inherent compressive strength, Lunar concrete made of KOHLS-1(Korea-Hanyang Lunar Simulant-1) is chosen as the structural material for the landing pads (Fig. 5a). The strength capacity of those pads was tested by JAXA (Fig. 5b), where results indicted adequate strength, suitable for several landing scenarios on the Lunar surface. Furthermore, the work of Kelso et al. [94] addresses construction of a 20-m-diameter vertical-takeoff-vertical-landing (VTVL) prototype pad (Fig. 6a), made of basalt material originated from the big island of Hawaii. The construction of such a pad constitutes a “proof of concept” project which demonstrates that a robotic precursor mission using rovers (rover Paver Deployment Mechanism-PDM) can construct a VTVL pad in a viable manner (Fig. 6b).

As mentioned above, a landing pad should create a safe zone for stable touchdown, leading to deflection of the exhaust plumes without creating a crater below the engine. These deflected plumes would scour the immediate area next to the central landing zone. Since the

Table 8
Chemical composition of the Martian original material and their simulants.

Oxide (wt%)	Original Martian material tested *in-situ* (Mean values)						Martian Simulants (Mean values or ranges)					
	Viking Landers		Pathfinder	Pathfinder	MER	MER	Made in US				Made in UK	Made in China
	1	2		Soil	MER-1/Oppy	MER-2/Spirit	JSC MARS-1	MMS-I	MMS-II	MGS-1	Y-Mars	JMSS-1
	(a)	(a)	(b)	(c)	(d)	(e)	(b)	(f)	(f)	(g)	(h)	(i)
SiO2	43	43	44	42	43.80	45.8	34.5–43.5	49.4	43.8	45.57	44.97	49.28
TiO2	0.66	0.56	1.1	0.80	1.08	0.81	3–3.8	1.09	0.83	0.30	0.77	1.78
Al2O3	7.3	7.0	7.5	10.30	8.60	10	18.5–23.3	17.1	13.07	9.43	13.31	13.64
Cr2O3	–	–	–	0.30	0.46	0.35	–	0.05	0.04	0.12	–	–
FeO	–	–	–	–	–	15.8	–	–	–	16.85	–	–
Fe2O3	18.5	17.8	16.5	21.70	15.60	–	12.4–15.6	10.87	18.37		7.57	16.00
MnO	–	–	–	0.30	0.36	0.31	0.2–0.3	0.17	0.13	0.10	0.18	0.14
MgO	6	6	7.0	7.30	7.10	9.3	2.7–3.4	6.08	6.66	16.50	14.32	6.35
CaO			5.6	6.10	6.67	6.1	4.9–6.2	10.45	7.98	4.03	7.65	7.56
Na2O	–	–	2.1	2.80	1.60	3.3	1.9–2.4	3..28	2.51	3.66	2.23	2.92
K2O	0.15	0.15	0.3	0.60	0.44	0.41	0.5–0.6	0.48	0.37	0.43	0.08	1.02
P2O5	–	–	–	0.70	0.83	0.84	0.7–0.9	0.17	0.13	0.37	0.09	0.3
BaO	–	–	–	–	–	–	–	–	–	–	–	–
NiO	–	–	–	–	–	–	–	–	–	–	–	–
SrO	–	–	–	–	–	–	–	–	–	–	–	–
SO3	6.6	8.1	4.9	6.00	5.57	5.82	–	0.10	6.11	2.63	–	–
Cl	0.7	0.5	0.5	0.90	0.44	0.53	–	–	–	–	–	–
H2O	–	–	–	–	–	–	–	–	–	–	–	–
Total	88.8	75.8	89.5	99.80	99.18	99.37		99.24	100.0	99.99		99.47

(a) Banin et al. (1992) [81] (b) Allen et al. (1998) [77] (c) Foley et al. (2003) [82] (d) Rieder et al. (2004) [83] (e) Gellert et al. (2004) [84] (f) Peters et al. (2008) [78] (g) Cannon et al. (2019) [85] (h) Stevens et al. (2018) [86] (i) Zeng et al. (2015) [80].

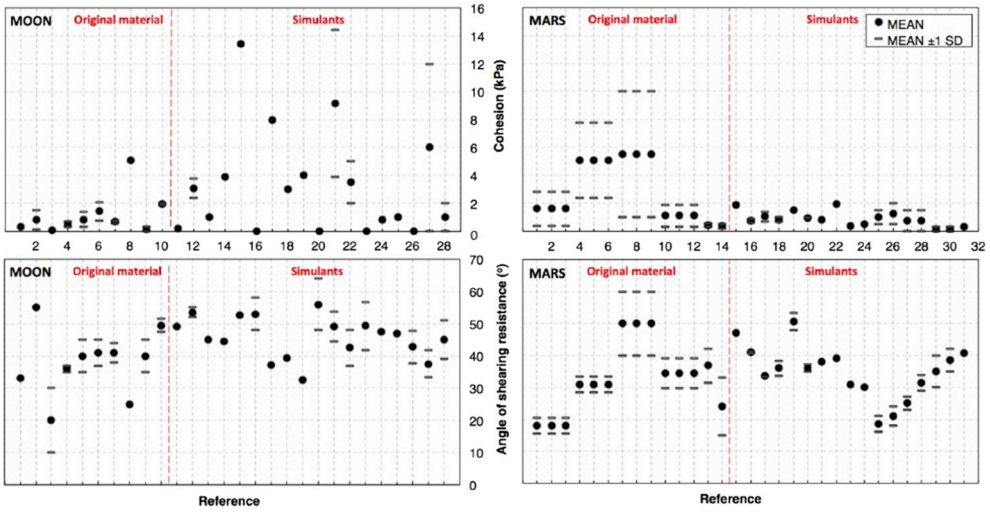

Fig. 2. Mechanical characteristics (cohesion up and angle of friction/shearing resistance down) for the original Lunar and Martian regolith along with the corresponding simulants. The box-and-whisker markers indicate mean values and ranges, where available from the original source. The x axis indicates bibliographical references as numbered in Table 9.

immediate area is substantially larger than the central landing area, it would be important to stabilize this area by using local materials. The work of Van Susante and Metzger [95] focuses on experiments on rock-stabilized zones and their layering. Additionally, these authors present a technique for in-situ construction of the necessary rock cover in order to lock the regolith dust. Furthermore, they discuss a method of evaluating the maximum rock size required for the stabilization of the underlying layers during take-off and touchdown of a rocket. Van Susante et al. [96] build upon Van Susante and Metzger [95] and discuss the option of using local rocks for constructing landing pads.

Apart from the fabrication of landing pads (as a monolithic base), there is great concern about how their smaller individual parts (tiles) would bind together. Thus, Ferguson et al. [97] investigate the creation of a nickel/aluminum (1:1 mol ratio) combustion joining, involving tiles made of Lunar regolith simulant (JSC-1A), through sintering techniques (Fig. 7). Additionally, Romo et al. [98] deviate from the previous concepts associated with 2D landing pads and present a design for 3D interlocking of tiles via a cellular tessellation system. The authors anticipate that beyond the construction of 2D landing pads, such a technique will have other applications including thermal control and protection from micrometeoric showers, radiation shielding, shade walls, road paving and other kinds of platforms. Finally, 3D-printed pads made of regolith tiles could play the role of rigid rafts for prospective extraterrestrial structures, substituting the typical foundation systems that would require (extensive) excavations. Leach et al. [99] highlight the merits of using Contour Crafting (CC) on the Lunar surface in order to fabricate not only landing pads and roads, but also blast walls, hangars and other critical parts of a habitat infrastructure.

Table 9
Numeration of the Lunar and Martian original samples and simulants.

	LUNAR REGOLITH				MARTIAN REGOLITH		
	n.a	Mission/Simulant	Reference		n.a	Mission/Simulant	Reference
ORIGINAL SAMPLES	1	Lunar Orbiter (1966)	Nordmeyer (1967) [29]	ORIGINAL SAMPLES	1	Viking Lander 1 (1975)	Moore et al. (1982) [69]
	2	Surveyor I (1966)	Jaffe (1967) [30]		2	Viking Lander 1 (1975)	Moore et al. (1987) [70]
	3	Lunar Orbiter (1966)	Moore (1970) [32]		3	Viking Lander 1 (1975)	Moore and Jakosky (1989) [67]
	4	Surveyor III and VI (1967)	Scott and Roberson (1969) [1]		4	Viking Lander 1 (1975)	Moore et al. (1982) [69]
	5	Apollo 11 (1969)	Costes et al. (1970) [33]		5	Viking Lander 1 (1975)	Moore et al. (1987) [70]
	6	Apollo 11 (1969)	Costes et al. (1971) [34]		6	Viking Lander 1 (1975)	Moore and Jakosky (1989) [67]
	7	Apollo 12 (1969)	Costes et al. (1971) [34]		7	Viking Lander 1&2 (1975)	Moore et al. (1982) [69]
	8	Luna-16 (1970)	Leonovich et al. (1974) [25]		8	Viking Lander 1&2 (1975)	Moore et al. (1987) [70]
	9	Apollo 14 (1971)	Mitchell et al. (1971b) [35]		9	Viking Lander 1&2 (1975)	Moore and Jakosky (1989) [67]
	10	Apollo 15 (1971)	Mitchell et al. (1972b) [36]		10	Viking Lander 2 (1975)	Moore et al. (1982) [69]
SIMULANTS	11	JSC-1	Perkins et al. (1991) [41]		11	Viking Lander 2 (1975)	Moore et al. (1987) [70]
	12	JSC-1	Carrier et al. (1991) [28]		12	Viking Lander 2 (1975)	Moore and Jakosky (1989) [67]
	13	JSC-1	McKay (1994) [42,43]		13	MPF Sojourner (1996)	Moore et al. (1999) [63]
	14	JSC-1	Klosky et al. (1996) [44]		14	MPF Sojourner (1996)	Moore et al. (1999) [63]
	15	JSC-1	Perkins and Madson (1996) [45]	SIMULANTS	15	JSC Mars-1	Allen et al. (1998) [77]
	16	MLS-1	Perkins and Madson (1996) [45]		16	JSC Mars-1	Perko et al. (2006) [76]
	17	FJS-1	Kanamori et al. (1998) [47]		17	JPL Lab 107	Perko et al. (2006) [76]
	18	FJS-2	Kanamori et al. (1998) [47]		18	JPL Lab 82	Perko et al. (2006) [76]
	19	FJS-3	Kanamori et al. (1998) [47]		19	MER Yard 317	Perko et al. (2006) [76]
	20	JSC-1	Klosky et al. (2000) [46]		20	MARS Yard	Perko et al. (2006) [76]
	21	JSC-1A	Klosky et al. (2000) [46]		21	MMS sand I	Peters et al. (2008) [78]
	22	JSC-1A	Alshibli and Hasan (2009) [46]		22	MMS sand II	Peters et al. (2008) [78]
	23	JSC-1A	Zeng et al. (2010) [49]		23	MMS dust I	Peters et al. (2008) [78]
	24	TJ-1	Jiang et al. (2012) [50]		24	MMS dust II	Peters et al. (2008) [78]
	25	TJ-2	Jiang et al. (2012) [50]		25	ES-1	Brunskill et al. (2011) [79]
	26	GRC-3	He et al. (2013) [51]		26	ES-1	Brunskill et al. (2011) [79]
	27	CAS-1	Lu and Jianguo (2014) [52]		27	ES-2	Brunskill et al. (2011) [79]
	28	BP-1	Suescun-Florez et al. (2015) [53]		28	ES-2	Brunskill et al. (2011) [79]
					29	ES-3	Brunskill et al. (2011) [79]
					30	ES-3	Brunskill et al. (2011) [79]
					31	JMSS-1	Zeng et al. (2015) [80]

3. Extraterrestrial ground motions and seismic hazard considerations

This paper continues with some basic elements of extraterrestrial seismology. Since ground motions on the Lunar/Martian surface, combined with the microgravity, could pose a hazard for potential extraterrestrial structures, we will briefly mention a few of the main findings based on the ground motions recorded on the moon. We note at the outset that this overview does not intend to capture or exhaust all results derived from the study of Lunar/Martian recordings, which span a very wide field of disciplines in geophysics and seismology and are not directly related to this paper.

It is observed that terrestrial planets (also known as telluric or rocky planets, i.e., having a solid surface and in contrast to gas planets) abide by the same structural framework in that they consist of a crust, mantle and core. These were developed after their formation and indicate their subsequent evolution. More specifically, the Moon is composed of a geochemically distinct crust, mantle and core and it is believed that its current structure was created by the fractional crystallization of a magma ocean following its formation, 4.5 billion years ago. Martian crust is 10–50 km thick, its mantle is likely 1240–1880 km thick, and its core likely has a radius between 1500 and 2100 km [21,61,62]. Many

Table 10
Summary of anchoring methods in extraterrestrial environments.

Anchoring & drilling technique	Description	Reference
Helical anchoring (Fig. 3a)	Focusing on the practicality of the helical anchoring method and its resistance to uplift; developed through experimental work performed on JSC-1 Lunar simulant.	Klosky et al. (1998) [87]
Suction drilling (Fig. 3b)	A drilling technique that takes advantage of pumping the grained soil out of the borehole by using cold gas flow. For the case of the Moon, the lack of atmosphere means the amount of gas needed for the drill should be included in the weight budget. On the other hand, the thin Martian atmosphere will provide an unlimited gas resource.	Kömle et al. (2008) [89]
Circular wedge anchoring (Fig. 3c)	Experimental study focusing on the assessment of the effect of circular wedge anchoring applied on a compacted Lunar simulant. The main goal is the establishment of verified anchoring standards (which can be applied to the design of Lunar facilities) through the development of a function between pull-out force and theoretical models of the failure mechanism.	Chang et al. (2010) [90]
Claw anchoring (Fig. 3d)	The proposed method uses the Discrete Element Method (DEM) for evaluating the perpendicular (with respect to the surface) and holding forces exhibited by claw anchoring. Both engagement and disengagement forces are referred to as perpendicular forces, since they are pointed into or out of the surface.	Ebert & Larochelle (2016) [91]

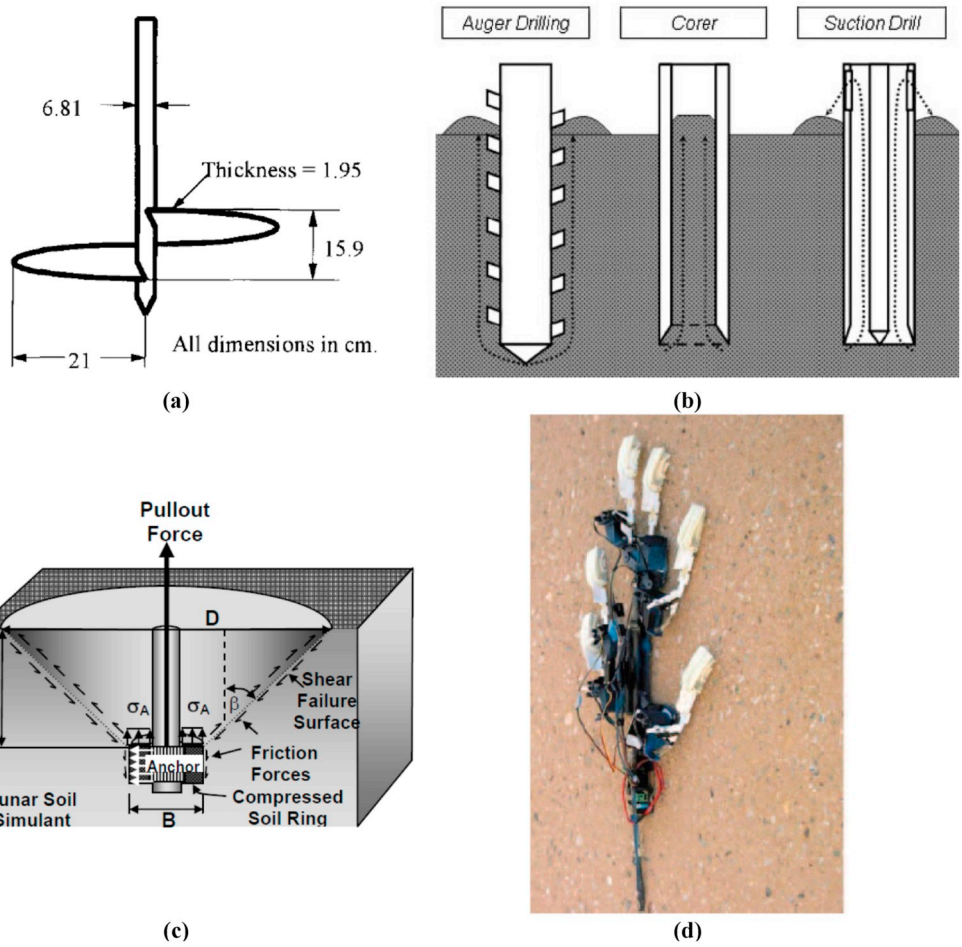

Fig. 3. Anchoring and drilling techniques. a) Helical anchoring, Klosky et al. [87]; b) Suction drilling, Kömle et al. [89]; c) Circular wedge anchoring, Chang et al. [90]; d) Claw anchoring, Ebert & Larochelle [91].

Fig. 4. Residual crater after solid motor firing is complete [92].

more details on its structure are currently being explored thanks to the Insight project underway in recent months.

Since the beginning of the planetary exploration era, seismology was considered a very useful tool towards understanding the characteristics of a celestial body and its interior. Seismometers were installed on the Lunar surface by astronauts of the Apollo 11, 12, 14, 15 and 16 missions from 1969 to 1972. The seismometers remained functional until their switch-off in 1977 [100], after which time similar data were never again recorded on the moon. During their operation, the seismometers were used for active and passive experiments, i.e., to record ground vibrations originating from man-made and natural sources respectively. At each seismometer location, four sensors/channels were deployed: three long-period sensors in the X, Y, and Z directions (LPX, LPY, LPZ), which recorded ground motion below 2 Hz, and one short-period sensor in the Z direction (SPZ), which recorded ground motion out to 10 Hz.

Over 12,000 events were recorded during the 8-year period of observation by the four seismometers installed on the moon [101], with newer ones discovered more recently by re-examining the data [102]. Over half of these remain unclassified. The natural sources of the recorded events were classified into four distinct types, namely: deep Moonquakes, shallow Moonquakes, thermal Moonquakes, and meteoroid impacts [103]. Fig. 8a shows some typical records for the different source categories, as recorded by each of the four sensors available per seismometer location. This is a well-known figure from Nakamura et al. [104] showing some of the strongest ground motions recorded; e.g. note that the LPY component of the meteoroid impact has clipped, i.e., reached its largest possible recordable amplitude. Note that one of the main characteristics of the recorded events are their very long durations; hence the compressed time scale in the figure, where 1 tick on the time axis corresponds to 10 min, leading to some recordings lasting over half an hour (as opposed to typical durations of a few minutes for earthquakes on Earth). It is important to mention at this point that all classified events in the catalogue were recorded at long distances, ranging roughly from 500 to 1200 km. This means that attenuation (both intrinsic and scattering) along the path from the event source to the recording site has played a significant (and difficult to

(a) (b)

Fig. 5. Use of KOHLS-1. a) Prototype tile; b) Compression strength tests [93].

quantify) role in decreasing the ground motion amplitude in all existing recordings.

3.1. Deep moonquakes

Deep Moonquakes are by far the most common classified natural source of ground motion, making up 3000 out of the 12,000 events in the Lunar database. They occur at large depths, approximately halfway between the Lunar surface and the Lunar center. The cause of these phenomena is mainly related to the tides generated on the moon due to the relative motions of the sun and the earth [106], although further studies may better clarify the mechanism. Deep Moonquakes have been detected from almost eighty repeating sources, at depths ranging from 700 to 1100 km [107]; to put this in perspective, consider that on Earth, deep earthquakes have foci ranging from 300 to 700 km, and much closer to the surface considering the Earth's larger 6371-km radius. Several hundreds of deep Moonquakes were recorded on an annual basis during the Apollo passive experiments, with a maximum magnitude of about 3 m_b [108]. Since the waveforms of individual Moonquakes generated at a certain source region were almost identical, the researchers were able to apply stacking techniques in order to improve the signal-to-noise ratio of seismograms by combining many co-located events [109]. It is noteworthy that this tendency for repetition and localization of deep moonquakes has been compared to similar tendencies of intermediate-depth earthquakes (i.e., with depths of 60–300 km) on Earth [110].

3.2. Shallow moonquakes

Of all the types of classified events, shallow Moonquakes (also known as high-frequency teleseismic events) are by far the rarest, with only 28 confirmed events in the entire database. However, they are the most seismically energetic phenomena observed on the moon [103], with a maximum estimated magnitude (in the admittedly very short 8-year observation period) of about 4.8 m_b [108]. The vast majority of those events occurs in the upper Lunar mantle [111] and their origin is not correlated with tidal effects, as is the case with deep Moonquakes. Shallow Moonquakes are considered representative of the potential tectonic quakes that would occur in the lithosphere of a single-plate planet. It has been considered [101] that shallow Moonquakes bear great resemblance with intraplate earthquakes, i.e., the earthquakes that take place in stable continental regions, as opposed to active shallow crustal earthquakes, which originate at plate boundaries. Their similarities involve their non-tidal character, their occurrence at locations of structural weakness, the ratios of small to large events (which

Fig. 7. Combustion joining of tiles [97].

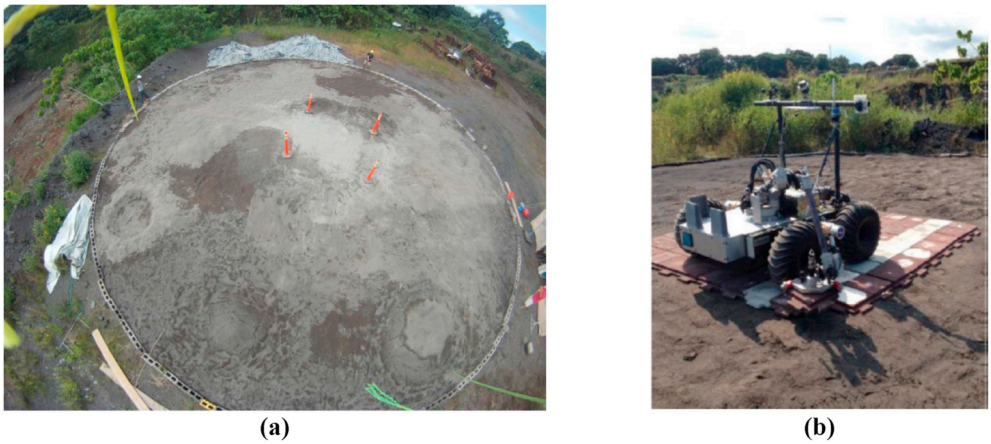

(a) (b)

Fig. 6. Proof of concept of the robotic construction of a 20-m VTVL landing pad. a) In-situ basalt Moon-scape; b) Paver deployment mechanism (PDM) [94].

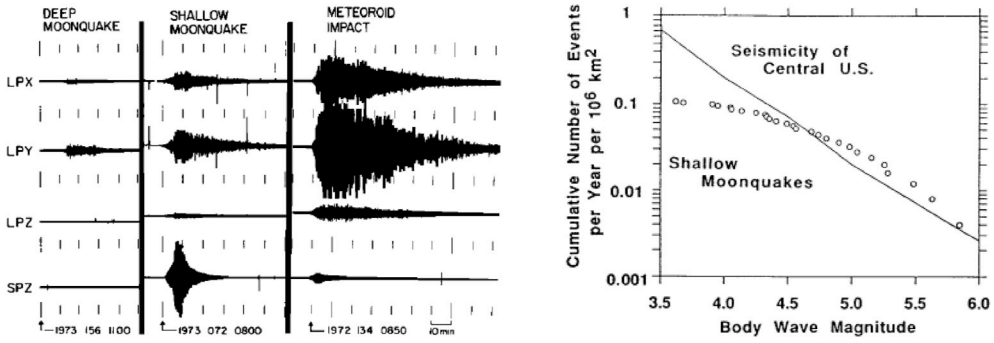

Fig. 8. a) Typical Lunar recordings in compressed time scale, namely: a deep moonquake (left), a shallow moonquake (middle) and a meteoroid impact (right) as recorded by the 4 sensors available at the S16 seismometer location (X,Y,Z on the long-period and Z on the short-period) [104]. b) Comparison of magnitude-frequency relationships for shallow moonquakes vs. intraplate earthquakes in Central US [105].

are related to the concept of seismicity rate), and the levels of activity [101].

Oberst & Nakamura [105] first considered the concept of seismic hazard and risk for a potential Lunar base. They showed similar seismicity rates for shallow moonquakes and intraplate earthquakes (Fig. 8b), which is a very interesting finding when considering the potential hazard of ET structures. They also considered the higher high-frequency content of the moonquakes, the lower attenuation of the Lunar crustal formations, the stronger scattering of the fractured Lunar surface, and the much longer durations of moonquakes. A rough estimate they made based on the occurrence rate was that a Lunar base constructed at a random location may be exposed to a shallow moonquake of magnitude above 4.5 m_b within a distance of 100 km once in 400 years. The very short observation period may not allow sophisticated estimates of probabilities of exceedance, but it is worth mentioning that regular (i.e., typical everyday buildings as opposed to critical infrastructure) structures on Earth are designed for seismic ground motion exceeding a certain level at a 10% probability in 50 years, which under certain conditions can correspond to a given design earthquake with a return period of 475 years.

3.3. Thermal moonquakes

Thermal Moonquakes are small local events caused due to temperature variations on the Lunar surface and can be detected up to a few kilometers (e.g. 4 km) away from the seismic stations [112]. A likely generation procedure of such seismic events is the movement of regolith in response to the diurnal changes in thermal stresses, and they can be related to large rocks and small craters [113]. Their signals can be almost identical and occur at specific times of the Lunar day. Based on their predictability and small amplitude, it is unlikely that thermal Moonquakes would pose a considerable threat to Lunar structures.

3.4. Meteorite impacts

Impacts do not originate from any internal Lunar procedure, and so they do not reflect the original Lunar seismicity. Nevertheless, such impacts were detected in abundance by the Lunar seismometers (over 1700 events in the 8-year recording period of the experiment) and constitute a rather important source of information accounting for the interplanetary environment [103]. They are also a consideration when it comes to natural hazards for Lunar structures. Contrary to the Earth, the Moon has no atmosphere and hence there is not enough hindrance to burn up falling meteoroids and prevent their impact on the surface; their average velocity reaching the moon is around 22.5 km/s [114]. Frequent impacts detected by short-period seismometers correspond to meteoroids of masses less than 0.5 kg [115], while rare events can be related to masses of over a ton, with diameters over 1.5 m [71]. Over 4000 impactors over 1 kg may strike the Lunar surface per year. The occurrence rate is difficult to predict and the signals can vary greatly as to amplitude and frequency [115]. As estimated from the seismic recordings, the impact points of large meteoroids are not uniformly distributed across the Lunar surface, but exhibit clustering [116]. A possible explanation for the creation of many of those clusters, as given by Dorman et al. [117]; is that they are related with known meteor showers. However, the largest events observed were outside shower periods and their occurrence seems related to when the moon is farthest away from the Earth [71]. Since the largest observed impactors do not belong to showers, nor are they predictable (as e.g. are thermal moonquakes), we consider meteor impacts a non-negligible source of hazard to lunar structures. The meteoroid-impact-related hazard is also visually evident through the Lunar Reconnaissance Orbiter Camera (LROC), whose data will help scientists to evaluate the history and current state of bombardment of the Lunar surface and will also guide lunar surface operations for decades to come [118].

At the end of this section on extraterrestrial seismic hazard, we mention in passing a few of the key findings at the time of writing (May 2020) from the ongoing InSight mission to Mars. Since SEIS started recording and transmitting data, it has been confirmed that marsquakes seem to be fewer and smaller than earthquakes. Despite the many sources of noise that render detection challenging (wind, lander vibrations, and variations in temperature, magnetic field and pressure), marsquakes are being detected. This is however possible mostly during the early evening hours, after the strong winds that dominate the daytime have ceased; this leaves large recording gaps during daytime. On April 16, 2020 there were 470 events in the InSight catalog, with 92 tectonic quakes having clear P- and S-wave arrivals and more events having no clear arrivals [119]. Some of the clearest marsquakes so far have magnitudes of 3.7 and 3.6 and were recorded at distances longer than 1500 km. These recordings have durations of 10 min or more, which compare well to similar-distance recordings on Earth (albeit from much larger events) and also have similar S–P arrival differences. The small observation period (9 months only, with most hours per day too noisy to record) does not allow a precise estimate of the seismicity rate, though there seems to be a gap in larger events [120]. The observed events till now are grouped into low-frequency events coming from the mantle, high-frequency (out to 8 Hz) and very-high-frequency (above 10 Hz) events coming from the crust, and super-high-frequency events likely related to thermal cracks. The high-frequency events exhibit seasonality, although its pattern is too complex to understand yet [121]. A 2.4-Hz resonance is observed systematically through the seismic events, which may be related to Martian structure [122]. So far, the attenuation on Mars seems to be roughly three times higher than on the Moon, with the upper 10 km being highly fractured or altered [123].

4. Extraterrestrial structures

Structural analysis and design in extraterrestrial (ET) environments is yet at a very early stage. Various researchers have proposed a plethora of concepts regarding different structural systems in ET environments through the years, but until now there is no complete or systematic study of structures. We believe this is due to a great extent to the uncertainties related to regolith, structural materials, ET natural

hazards and construction methods. At this point, it is worth mentioning that a novel proposal for the potential location of future permanent habitats are Lunar or Martian lava tubes, as proposed by Theinat et al. [124]. In this case, the underground habitat would be fully protected from the harsh surficial hazards (e.g. solar radiation and meteoroid impacts). Theinat et al. [125] have conducted both analytical and numerical analyses incorporating different sizes of lava tubes and different material properties, in an effort to investigate their stability.

A first attempt to categorize ET structures was made by Cohen [126]; who grouped them in three different classes based on: (a) site features, (b) structural concepts and (c) habitable functions. Following Cohen's class (b), this paper focuses on the most popular concepts for constructing ET structures, which so far are:

- Inflatable structures: Inflatable dome-shaped structures appear to be the most prevalent structural systems, since (a) they can effectively withstand high tensile forces as a result of the expected internal pressures, and (b) before inflation they occupy minimal space and therefore can be easily transported.
- Deployable structures: Deployable structures constitute another popular solution for space exploration, since they can easily deploy from their initial state that occupies minimal space and thus they can be compactly stowed during their transportation. However, until now, most deployable applications focus on small, lightweight structures such as antennae, which are out of the scope of this paper.
- 3D-printed structures: Given that material transportation from the Earth would have severe cost and volume limitations, the in-situ resource utilization (ISRU) framework is very appealing. ISRU suggests utilizing indigenous material (i.e., regolith) combined with robotics in order to effectively construct the first ET structures [127]. The idea of 3D-printed regolith-based structures is based on the assumption that Lunar and Martian regolith can exhibit desirable structural properties when treated appropriately.

4.1. Generic structural concepts

We have decided to present the various types of structures leading with a subsection of more general, conceptual approaches. The authors here focus only on different structural typologies and therefore their approaches do not fit under any of the three aforementioned categories. Although some of the proposed ideas are pioneering and innovative, they may not consider the construction method, the lack of structural material resources on-site, or a specific foundation system in their approach. The proposed ideas are presented in chronological order, to show the evolution of the engineering way of thinking over time.

Benaroya & nagurka (1990) [128]

Through a selective technical overview on the vibration and control of large-space structures (e.g., low-stiffness precision-shaped antennas, low-stiffness planar structures for large solar arrays, high-stiffness trusses for space facilities and platforms, Lunar bases, etc.), the authors summarize some technical challenges that engineers will encounter during and after the design of such structures. The first part of the paper introduces the large-space structures and discusses issues pertaining to their dynamics, while the second part examines structural control aspects, including the design of a control system using linear state-space techniques.

Benaroya & Ettouney (1992a) [129]

This paper presents a quantitative framework resulting in a generic but optimal structural type, addressing the most critical parameters of ET structural design. The approach involves a numerical example of a flat 3D truss structure supporting a regolith shield that protects the habitat from extreme temperature fluctuations and extreme radiation, as shown in Fig. 9. The assumed loading is: (a) gravitational forces from the self-weight of the structure and regolith shielding, and (b) internal pressures. The study, after implementing a linear static analysis, concludes as to the optimal structural weight of the truss against both its maximum length and spacing, when the maximum height of the regolith shield varies. The study also incorporates some preliminary cost analysis.

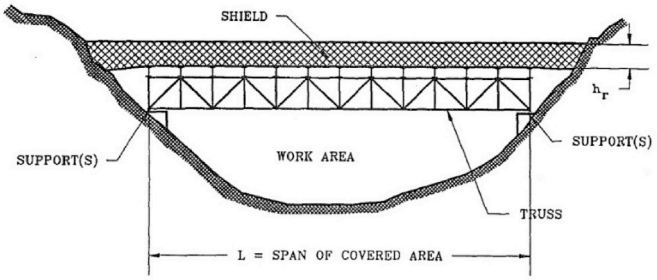

Fig. 9. Flat truss/trench Lunar base concept, Benaroya & Ettouney [129].

Benaroya & Ettouney (1992b) [130]

This paper discusses a way to automate engineering processes for a Lunar outpost facility. More specifically, it attempts to adjust a number of important design rules stipulated by the American Institute of Steel Constructions (AISC) to Lunar environmental conditions. The issues discussed in this project are related to: (a) scaling of loading due to low gravity, (b) fatigue and thermal cycling effects, (c) the probability of brittle fracture due to extremely low temperatures (d) the adjustment of the (originally developed for considering the uncertainties in design/construction on Earth) safety factors, to the new Lunar environmental requirements, (e) adjusting the buckling, stiffening and bracing requirements to the Lunar gravitational conditions taking the internal pressure into account and (f) the consideration of new failure modes such as high-velocity micrometeorite impacts.

Ettouney et al. (1992) [131]

Three types of cable structures are described in this paper: (a) small-span, (b) medium-span, and (c) large-span structures. The paper concludes that for small spans it is ideal to use a reinforced cable system along with a three-hinge arch, while for medium spans a pre-tensioned cable system would be more appropriate. Finally, for longer spans, pre-tensioning cables together with a stiffened truss are suggested. It is also shown that foundations for these structures may experience uplift, but with a small alteration of the cable system the problem may be addressed and lead to lower cost, improved system behavior, and substantially reduced manpower involvement.

Benaroya (1993) [132]

This paper presents a thorough overview of various tensegrity structural suggested as case studies for possible use as Lunar structures. The tensegrity concept refers to a system consisting of bars and cable nets which obtains a standard geometry and stiffness when the bars are in compression due to the tension in the cable net (Fig. 10). The reported advantages of tensegrity structures are: (a) they are self-sustaining, thus there is no need for complex anchoring or deep foundations, and (b) they are independent of the internal pressure (contrary to inflatable structures, described in section 4.2). However, their main disadvantages are related to their construction and transportation from Earth. Furthermore, this work includes a preliminary design of a pre-stressed tensegrity structure through static analysis, considering the required prestressing forces and constraints of member deformation.

Jolly et al. (1994) [133]

A preliminary design is proposed for a Lunar outpost shelter, as shown in Fig. 11. The proposed structure is based on similar concepts as the ones mentioned above: that is, a regolith shelter depending on the excavation depth supported by a truss (made of a composite material) structure. It is reported that the depth of excavation will be designated according to various ET natural hazards such as meteoroid showers, galactic cosmic radiation (GCR), solar proton events, and extreme temperature fluctuations. This paper focuses especially on the need to take into account the meteoroid impacts on a shelter and elaborates on their probability of occurrence versus their mass. An interesting point is that this is the first paper to ever propose centrifuge testing using similitude scaling relations to model low gravity.

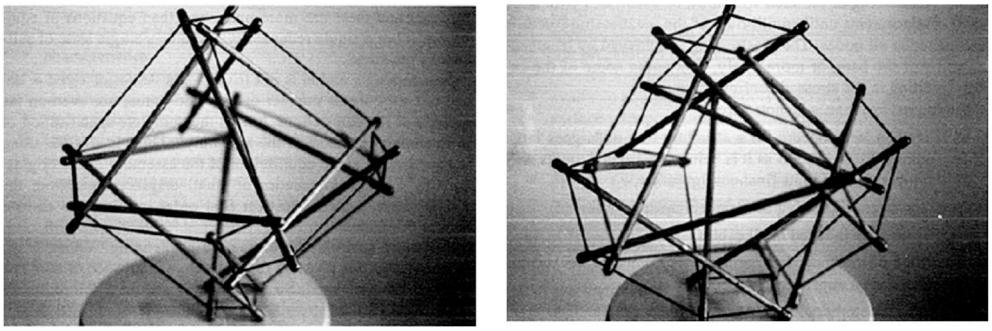

Fig. 10. Various tensegrity structural concepts incorporating bars and cable nets [132].

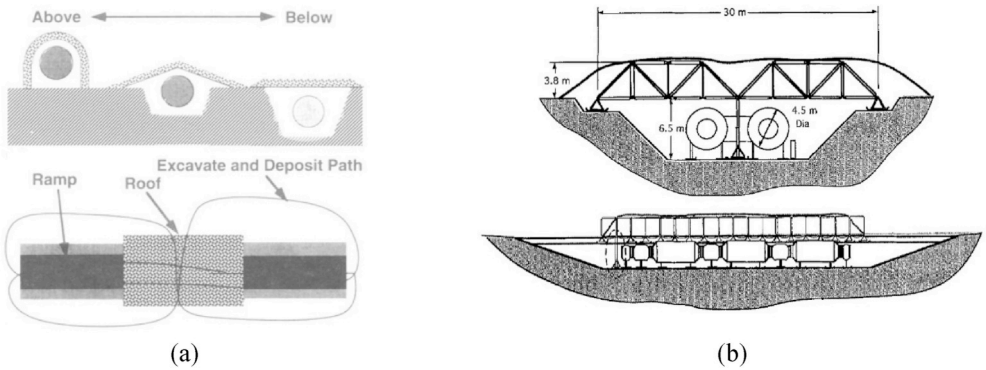

Fig. 11. a) Shielding concepts according to the depth of excavation; b) Large double truss suspends regolith shielding above habitats, Jolly et al. [133].

Malla et al. (1995) [134]

This work presents a design methodology to be implemented for the preliminary design of braced double-skinned long-span roof structures on the Moon. The idea proposed is to use a protective layer from regolith supported by a roof with a top and bottom plate, and between them a flat 3D truss core (made of aluminum), as shown in Fig. 12. To this end, the authors use analytical solutions (the Navier's and Levy's plate solutions), and in order to verify the accuracy of the design procedure they performed a linear static finite element analysis. The optimization of the braced double-skinned roof assembly shape is validated by the results of extensive parametric studies, considering realistic static loading such as pressurization, shielding and dead loads (lighting, heating, ventilation, etc.). Furthermore, the natural frequencies of the proposed roof structure are computed with a simplified method and compared with those of the finite element analysis.

Aulesa et al. (2000) [6]

With a view to minimizing the amount of Lunar structural materials required for the construction of a Lunar base, this work proposes a hemispherical shell structure (dome) following the in-situ resources utilization (ISRU) framework, as shown in Fig. 13. Therefore, the proposed structural material is cast basalt as it can be found on the Lunar surface. It is also noted that, as a buried structure, the base is characterized by a geometry that improves the distribution of active stresses (since -as a dome-it translates the gravitational loading to circumferential stresses and transfers them safely to the ground), while it also provides shielding/protection from the extreme ET conditions. More specifically, this structure is designed to support a dead load of 5.4 m of regolith shielding and to act as a permanent habitat for a crew of six people.

Benaroya (2006) [135] & ruess et al. (2006) [136]

The papers present and discuss structural concepts and possible materials for second-generation structures on the Moon (inflatable, cable or rigid and underground structures). Various different concepts are considered and the most rational is selected for design. More specifically, since gravitational loads govern the design on Earth, parabolic

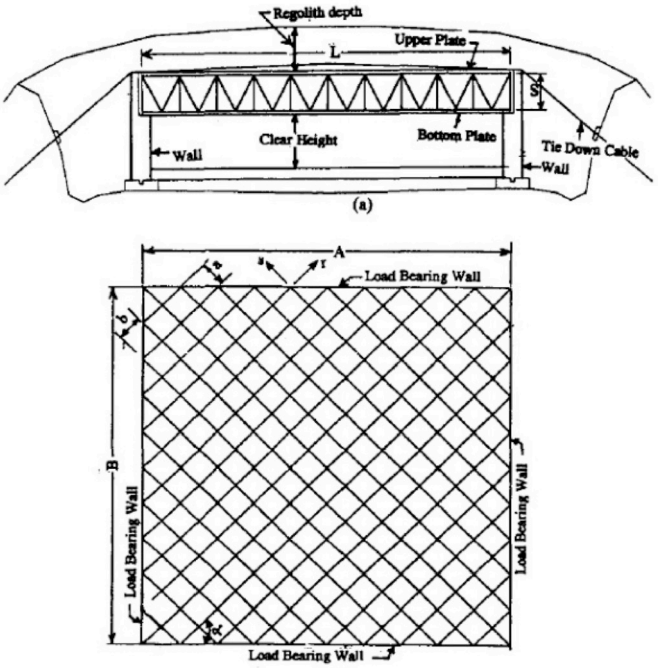

Fig. 12. Proposed double-skinned roof structure supporting a regolith cover, Malla et al. [134].

arches are preferred to semicircular as they minimize the potential for internal moments to develop. On the contrary, since on the Moon the internal pressure is more dominant than gravitational loading, semicircular arches are better for transferring the loads to the ground with minimum moments. Hence, the proposed structure is a semicircular arch, as shown in Fig. 14. The design is done by means of linear static

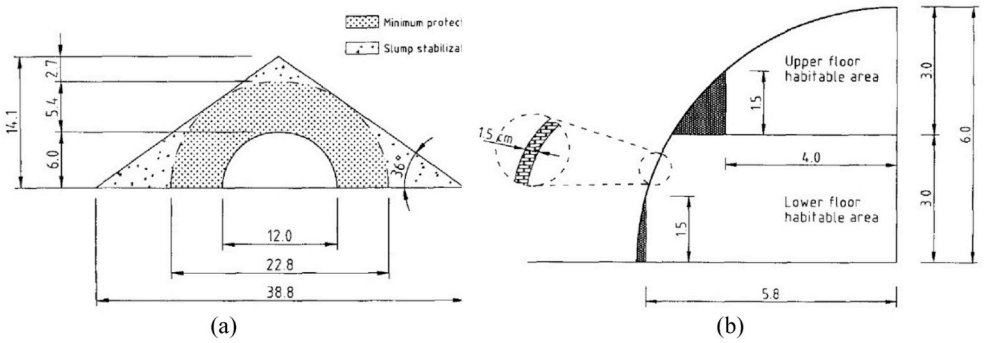

Fig. 13. a) Dimensioning of shell and regolith cover of a Lunar habitat for six people; b) minimum thickness of the cast basalt shell, Aulesa et al. [6].

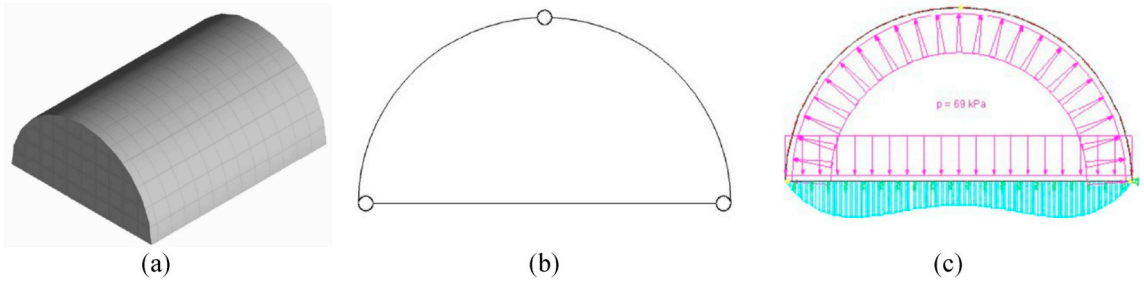

Fig. 14. a) Rendering of a Lunar habitat module; b) a three-hinged arch as a cross-section of the module; c) internal pressure and floor loading applied to the semicircular arch, Benaroya [135] & Ruess et al. [136].

finite-element analysis, considering: (a) high internal pressure, (b) floor loads, (c) regolith cover, (d) installation loads, (e) half the regolith cover during construction and (f) other dead loads.

Malla & Chaudhuri (2006) [137]

This paper proposes a potential Lunar structure simulated by a 3D aluminum frame (with tubular cross-sections) linked with an inflatable Kevlar membrane, as shown in Fig. 15a. Interestingly, this study considers a combination of different structural systems that resist both the internal pressures (membrane) and the 1.5 m regolith cover along with the dead loads. The stresses and deformations are calculated with static finite-element analysis. As is stated before, the layer of Lunar regolith offers protection from solar radiation, extreme temperature fluctuations and micrometeoroid impacts. The study also deals with two different cases of support conditions; either pinned connections or pins and roller supports.

Meyers & Toutanji (2007) [138]

This study focuses on three different types of structures made of "waterless" concrete within the ISRU framework: (a) a hemispherical dome; (b) a cylindrical structure; and (c) an arched panel structure. The concrete is made of sulfur, which is a by-product of oxygen and carbon. The authors claim that sulfur regolith concrete is an ideal material for building structures in a Lunar environment, since it can be found in abundance on the Lunar surface, while it exhibits high levels of strength and durability. Also, regolith-derived glass rebars and fibers can be combined with the regolith concrete to provide reinforcement. The main loading assumptions in this study are the high internal pressures and the temperature fluctuations. The final suggestions include solutions such as prestressed tendons across the arch or hinge joints at the arch crown, as shown in Fig. 16.

Malla & Chaudhuri (2008) [139]; Malla & Gionet (2016) [140]

Building upon the work of Malla & Chaudhuri [137]; this project presents the same concept of the 3D frame-membrane structure covered with regolith shielding and pressurized internally as a possible Lunar habitat. However, the focus now is on the dynamic behavior of the structure when subjected to a meteorite impact. Further results for the structural behavior obtained through dynamic impact analysis using nonlinear finite elements and considering large displacements are presented. For a more refined analysis, the study considers the added mass of the regolith and the stress-stiffening due to the high internal pressure load. This study is enhanced further in Malla & Gionet [140];

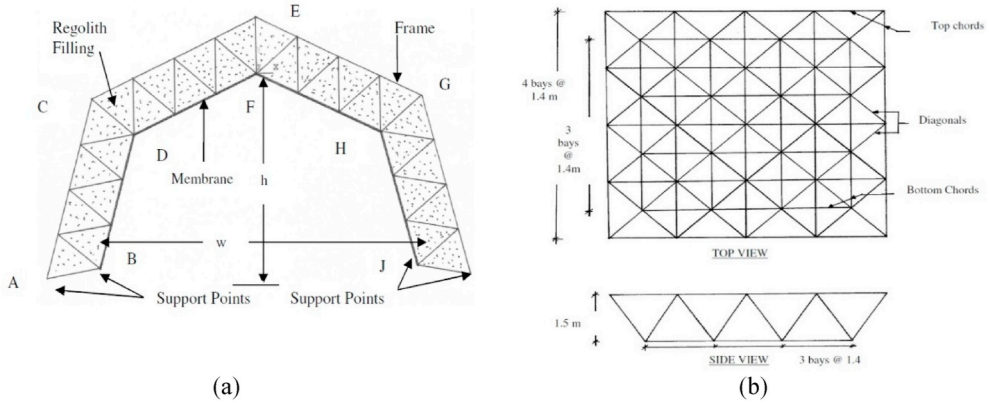

Fig. 15. Proposed structure: a) Elevation; b) Plan and side views, Malla & Chaudhuri [137].

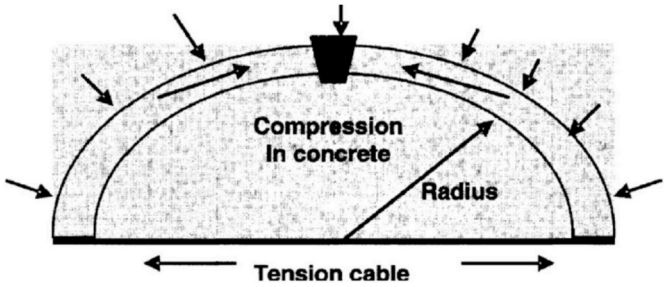

Fig. 16. Wall segment cross section of the proposed arch-shaped structure, Meyers & Toutanji [138].

where the authors increase the level of detail of the loading (pressurization, additional mass, impact) and consider the construction process as well. They find that the generated stresses due to the impact are significant only in the vicinity of the instantaneous applied loading (mid-point of a beam in the frame structure), while the static loading dominates all other areas of the structure. These studies were the earliest that considered a detailed dynamic analysis of ET structures.

Faierson et al. (2010) [141]

This study investigates the design of a Lunar physical asset within an ISRU framework. By utilizing a geothemite reaction (i.e., a reaction between minerals and a reducing agent) of a mixture of Lunar regolith simulants (JSC-1AF and JSC-1A) with aluminum powder, the authors claim that a regolith-derived voussoir dome can be constructed, as shown in Fig. 17a. More specifically, forming of the voussoirs is accomplished during the reaction by utilizing a fabricated silica-slip crucible to contain the geothermite reactant mixture (Fig. 17c). Thus, the product of the reaction assumes the shape of the crucible. The authors state that the design of the voussoir domes will depend mainly upon static stability rather than material strength. To this end, the horizontal thrust of a lune -an imaginary slice of the dome (see Fig. 17b)- is derived by means of static equilibrium (considering the dome weight) and it is shown that it must be counteracted by a tension element or an abutment-like structure.

Mottaghi & Benaroya (2015a) [142]: part I

This mature study is inspired by Ruess et al. [136]; proposing an igloo-shaped, magnesium-alloy structure founded on a 1-m sintered regolith raft with a 3-m regolith shielding, as shown in Fig. 18a. As stated before, this regolith cover accounts for protection from both radiation and temperature fluctuations based on Duke et al. (1985) and Vaniman et al. (1991), respectively. Fig. 18b shows the equivalent static pressures from the considered assumptions (regolith cover, magnesium structure, internal pressures). Furthermore, the difference is evident between the radial distribution of the internal pressures that results in a semicircular shape compared to the vertical uniform distribution of the gravitational forces that favor a parabolic shape. The paper conducts a detailed thermal analysis and concludes as to the fact that 3 m of regolith is sufficient insulation against the extreme Lunar temperature fluctuations.

Mottaghi & Benaroya (2015b) [143]: part II

Following the interesting work of Part I, this project continues with a preliminary seismic analysis of the structure proposed in Fig. 18. Given that, during the Apollo missions, shallow moonquakes with estimated body wave magnitudes of m_b 5.5 or more were observed [105,144], the authors deemed essential to consider the effect of larger Lunar seismic events to the structure. To this end, a seismic event with m_b 7 was generated based on the diffusion of a pulse in a heterogeneous medium and applied as stationary input to the structure, which was modeled and analyzed with finite element software (using 179,610 elements). As a first step, a static and modal analysis (considering zero damping) were performed. Then, the numerical analysis was conducted using a random vibration solver (ANSYS 14.0) that neglects the static stress distribution and calculates the von Mises stress. The results indicate that the risk associated with these events is low because this type of structures would be designed with a relatively high factor of safety and it is envisioned that due to the regolith-structure interaction they will exhibit high values of damping.

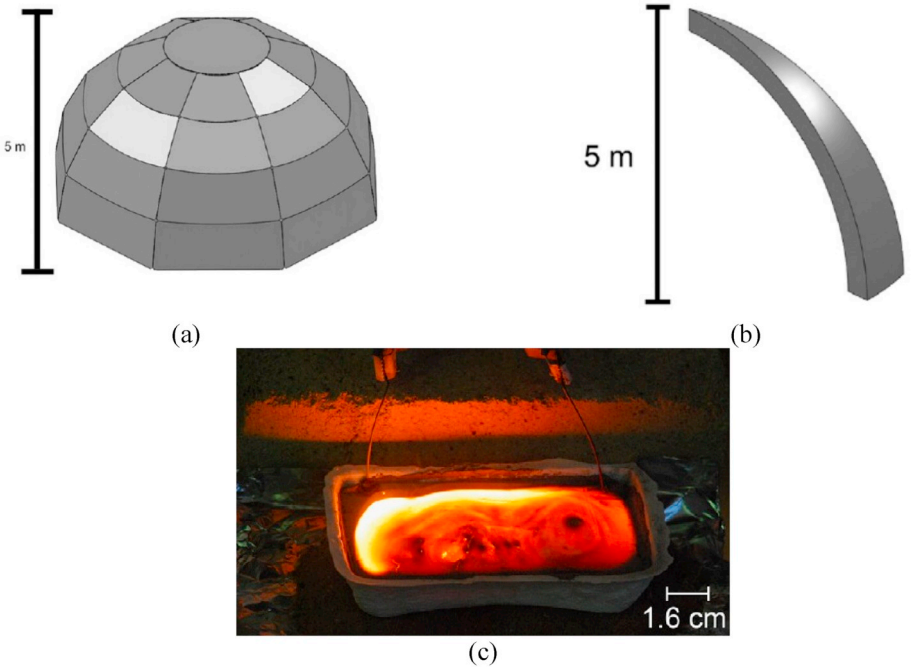

Fig. 17. a) Dome made by regolith-based voussoirs following a geothemite reaction; b) Lune geometry; c) Geothermite reaction using JSC-1A regolith stimulant, Faierson et al. [141].

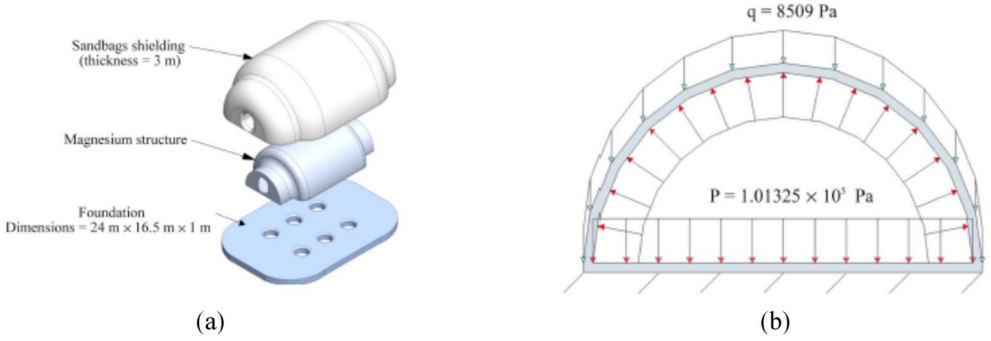

Fig. 18. a) Geometry of the proposed igloo-shaped structure; b) static pressures considered in a cross-section of the structure, Mottaghi & Benaroya [142].

Fig. 19. Toroid inflatable station concept during testing (NASA 1961), Courtesy: NASA.

4.2. Inflatable structures

A very specific structural category, inflatable structures, dominated the way of thinking of many pioneering engineers, since they are lightweight pressurized structures able to withstand extreme environmental conditions, and their volume increases according to the internal pressure. Such structures have frequently been proposed to support space applications by providing increased volume given a constant mass. In 1961, the first inflatable space habitat was design and constructed by Goodyear [145,146] as it is shown in Fig. 19. The concept of inflatable structures revived in 1989 with a proposal released by Johnson Space Center's Man Systems Division. It presented an 8m-radius Lunar outpost of spherical shape, designed to be partially embedded in the surface of the Moon. From 1989 onwards, the concept of inflatable structures started gaining popularity. A selection of these publications is presented below.

Nowak et al. (1992) [147]

This work addresses a modular inflatable structure -initially proposed by Vanderbilt et al. [148]- made of thin kevlar membranes (Fig. 20), for future use in a Lunar environment. The selected size of the preliminary module is $6.1mx6.1mx3.0m$, with the roof membrane having a radius of curvature 6.1 m. The results of the linear elastic analysis considering gravitational loads from the 3.3-m regolith shielding, the dead loads of the structural elements, and the internal pressure indicated that such structures are feasible for a Lunar base. More specifically, a roof membrane of 0.3 mm thickness combined with a 1.94 mm column membrane thickness would be sufficient. Furthermore, the authors present a nonlinear analysis (for large deformations) based on the cubic Bezier functions, to generate the optimum geometries of the proposed inflatable structures. Then, simulated results are used for the production of 3D wire frames and solid renderings of the individual components of the inflatable structure. The components are connected into modules, which can then be assembled into larger structures, based on the desired architecture.

Sadeh & Criswell (1993) [149]

In the same manner as Nowak et al. [147]; i.e., without focusing on the geometric modeling, these authors present preliminary calculations considering the design of a generic Lunar inflatable structure. More specifically, a single-level inflatable structure consisting of modules is proposed (Fig. 21). Each module is formed of a roof and subfloor kevlar membrane, four-side wall membranes of a doubly-curved prismoid shape, and an inflatable frame system. The inflatable frame system comprises four tubular columns (which are in tension as they hold the subfloor and the roof together) and four upper and lower tubular arches (which are in compression in order to equilibrate the membrane tension acting on them). The aim of this project is to evaluate the required thicknesses of the membranes. The results of the linear elastic analysis (subfloor membranes: 0.30 mm, sidewall membrane: 0.46 mm diameter of the inflatable tubular columns and arches: 0.46 mm) indicated that the structure could be suitable for the Lunar environment. The preliminary analysis considered gravitational loads from the 3-m regolith

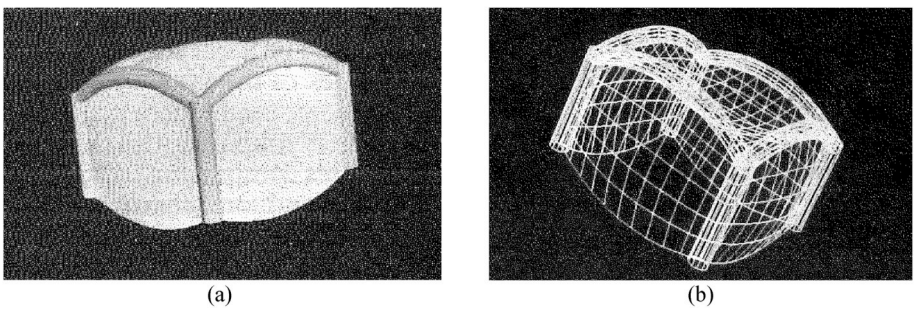

Fig. 20. a) Proposed inflatable module with Kevlar membranes, columns and arched ribs; b) wireframe of the inflatable module, Nowak et al. [147].

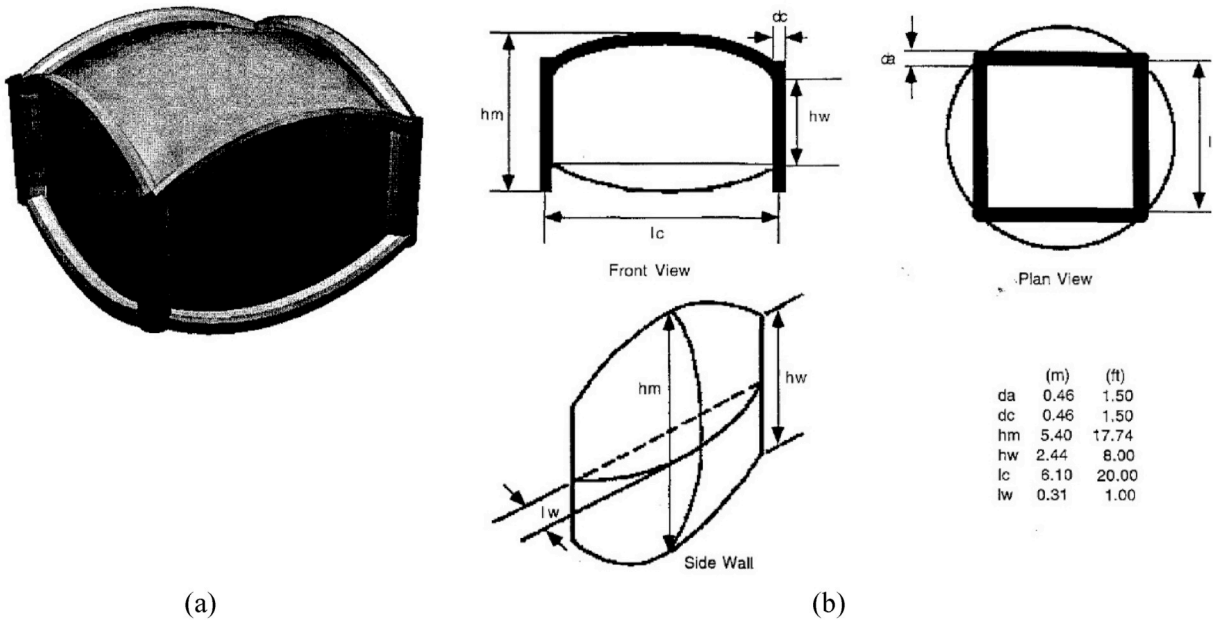

Fig. 21. a) Solid rendering of a module; b) major dimensions of the inflated module, Sadeh & Criswell [149].

shielding (about 8.77 kPa), the dead loads of the structural elements, and the internal pressure.

Abarbanel et al. (1996) [150]

This paper presents an analysis of a framing system to evaluate the optimum shape of an inflatable structure destined as a Lunar/Martian base, as shown in Fig. 21. The single module has a geometry of $(6.1mx6.1mx2.44m)$ and its material properties are described as: fabric Kevlar 49, $E = 38GPa$, $f_y = 690MPa$. The minimum thicknesses of the roof, subfloor and sidewall membranes are found to be 0.3 mm, 0.33 mm and 0.46 mm respectively. Furthermore, this project compares three different options regarding the framing system, which comprises 8 upper and lower cylindrical arches and 4 columns with 0.46-m diameter: (a) rigid thin-walled tubes; (b) iridized foam placed inside the membrane sleeves; (c) pressurized membrane tubes. The results of the finite element structural analysis highlight the supremacy of the third option, which meets structural requirements while at the same time being the most lightweight structure. The pressurized membrane tubes need a 0.77 m thickness filled with pressurized air to 900 kPa. The loads considered are the weight of the 3 m regolith shielding and internal pressures of 69 kPa, since the dead and live loads are negligible compared to them.

Cadogan et al. (1999) [151]

The authors present a review of past projects that focus on the design and manufacturing of inflatable structures. It is noted that the most important advantage of inflatable structures is their ability to occupy small volumes during their transportation from Earth. This leads to a significantly lower budget and allows for smaller launch systems to be used. Furthermore, the paper highlights the significance of the rigidization technologies, which will give the structural layer the ability to: (a) deploy in a flexible state, (b) become a rigid structural composite after the deployment and (c) enhance its structural capacity.

Kennedy (1999) [152]

This paper presents a description of TransHab as a potential habitation module for the International Space Station (ISS). TransHab is a hybrid space structure that consists of a hard central core and an inflatable exterior cell, as shown in Fig. 22. Additionally, TransHab utilizes mechanical connections to connect the reinforced carbon composite (Kevlar) structure with the woven pressure shell. The innovation here, compared to previously proposed structures, is that there is no more a single pressurized unit that acts as the main structure, but the main goal of this project is to provide a habitat for long-duration space missions, addressing all requirements known from prior experience (e.g., unique technology, high level of habitability).

Bateman et al. (2000) [153]

This work elaborates on the structural framing system demands required by the geometry of a “tuft pillow” inflatable structure (Fig. 21b), in order to optimize its structural behavior without altering the functionality of its design. Two different framing systems are examined in order to withstand combinations of tensile, compressive and flexural loads: (a) rigid thin-shell tubes made of a lightweight and strong material such as titanium and graphite/epoxy, and (b) pressurized membrane tubes made of Kevlar, since the membrane elements are pre-tensioned by the added pressure. Two modifications are proposed: (1) adding “ovaling and bending webs” (Fig. 23) to the column and arch members for reducing deflections and essentially increasing the resistance to the out-of-plane pulling and bending of the membrane; (2) “inclined tensioned tie-downs” added to reduce horizontal displacements at the top of the columns since their top displacements were not minimized with the first solution. The analysis is done with the ABAQUS software where the framing system is exposed to a combination of bending and axial loads from gravity and internal pressure.

Harris & Kennedy (2000) [154]

A filament winding method is proposed by NASA for the construction of large-scale inflatable structures appropriate for space applications. In particular, winding techniques suitable for constructing structures of great flexibility, constrained by an elastomeric matrix, employ tapes or tows of fiber wound around a mandrel at specific angles and locations, creating two general sets of fiber paths, namely: (a) bias fibers and (b) axial fibers. By employing bias angles greater than a certain equilibrium angle (which is related to the material and the shape of a structure), the structure will experience a tensile force while being pressurized. On the other hand, for a bias angle lower than the equilibrium angle, the structure will experience a contraction force while being pressurized. The proposed model (Fig. 24a) is analyzed by means of FEA. The bias angle was chosen equal to 67°. The ability of such structures to provide significant living space is also addressed, and the inflatable space habitat is identified as the most prevalent structural technology in extraterrestrial environments.

Jenkins and tampi (2000) [155]

This work initially provides some background in relation to the

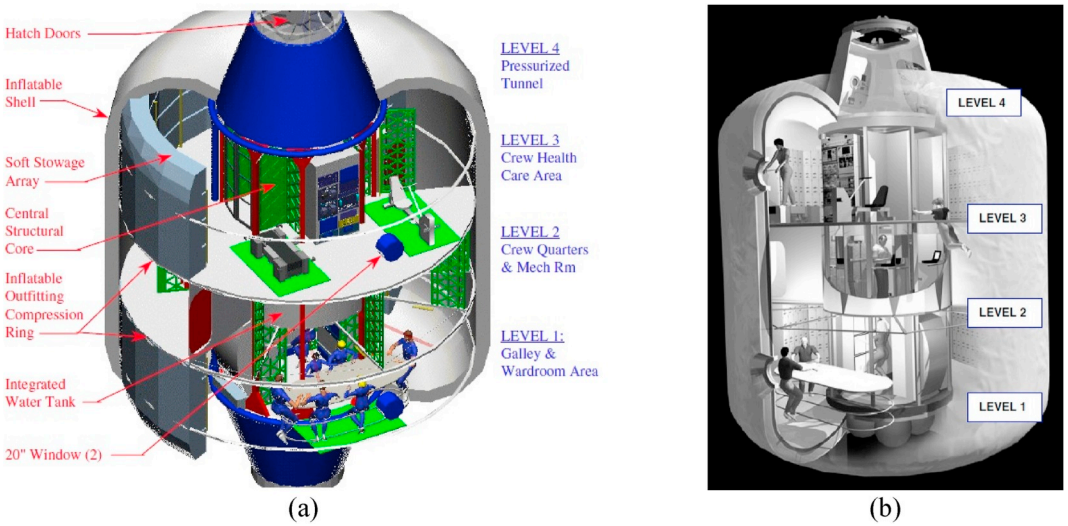

Fig. 22. a) TransHub overview; b) ISS Transhab internal view, NASA JSC S99-05363, Kennedy [152].

shape (deformation) control of membranes in inflatable structures. It also presents experimental results from vibrating circular membranes generated by a non-contact scanning laser vibrometer. Observing the results, the authors conclude that due to its low flexural stiffness, the membrane provides very weak transmission of bending information (as detected by the scanner) spatially. Nevertheless, the spatial spread of this information is strongly related to the membrane's tension and local curvature, among other parameters. Finally, an experimental investigation of the circular membrane is performed by means of dynamic analysis with appropriate boundary conditions (Mierovich, 1997). The authors conclude that, for lower frequency inputs, there is no discernible vibration response. However, at higher frequency inputs, the amplitude of the response increases abruptly.

Borin & Fiscelli (2004) [156]

This paper discusses various approaches and considerations on the design of a particular inflatable structural concept called the “Astrophytum”. Contrary to other approaches, the aim of this project is to design an astronaut-friendly environment inside the “Astrophytum” (Fig. 25a), able to accommodate 8 persons for 90 days in low Earth orbit. The five layers of the shell are: (a) an inner liner of Nomex and Kevlar, (b) a triple redundant bladder in Combitherm (each of them covered with Kevlar), (c) a restraint layer of Kevlar, (d) a shield for micrometeoroids and orbital debris in Nextel and expansive foam, (e) a Multi-layered insulation (MLI) -to endure extreme temperatures-in aluminized Mylar, combined with a multilayer of betaglass as protection from the atomic oxygen.

Criswell & Carlson (2004) [157]

This work describes the conceptual design for an economical structural configuration securing efficiency, reliability and functionality. More specifically, the project deals with a modular system based on three-level inflatable modules (top level for living space, middle level for operations and lower level for labs, with storage and equipment) of spherical (9-m diameter) shape (Fig. 26a), connected by mating rings (Fig. 26b). A multi-layered Kevlar membrane covers each module, providing structural containment and preserving the internal pressure levels. The project is supported by preliminary static analysis (mainly considering the internal pressure) and computer-generated visualization.

Adams & Petrov (2006) [158]

This project presents the design of a Surface Endoskeletal Inflatable Module (SEIM) (Fig. 27) that adopts two aspects from the TransHab [152] module technology: (a) the operational concept, but accounting for different conditions, such as the surface of an extraterrestrial environment; (b) streamlining the relationship between the hard and membranous structures which constitute this module's principal components. Moreover, the project proposes innovations regarding the design of a hybrid inflatable module which are related to: (1) the potential of supporting a non-metallic structure of the same capabilities; (2) the bypassing of the mechanical connectors by adding joining restraint layer straps directly to the core (Fig. 27a); and (3) the increase of the design flexibility of habitable hybrid inflatables, as shown in Fig. 27.

Brandt-Olsen et al. (2018) [159]

This project describes the various environmental parameters on Mars and identifies structural internal pressure as the dominating load, as shown in Fig. 28a. An iterative form-finding analysis of the pneumatic membrane structure is conducted by means of “Rhino/Grasshopper” software, using the “Kangaroo” plugin to account for the physics (Fig. 29). Various structural solutions are investigated (Fig. 28b). Thus, a shape catalogue for prospective solutions is proposed. The authors conclude that a hybrid material solution -Kevlar cable net combined with Ethylene tetrafluroethylene (ETFE)

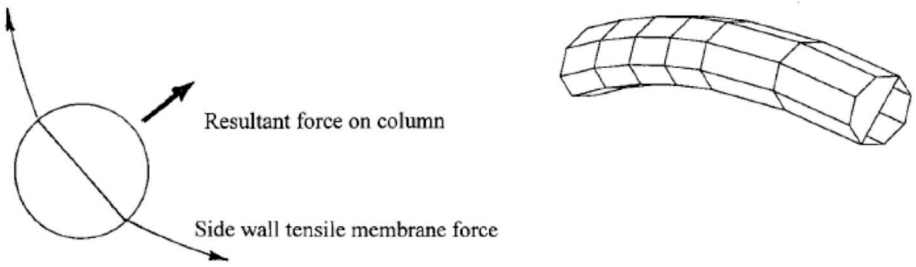

Fig. 23. a) Cross-section of the columns and arch members having an ovaling web; b) the ovaling web, Bateman et al. [153].

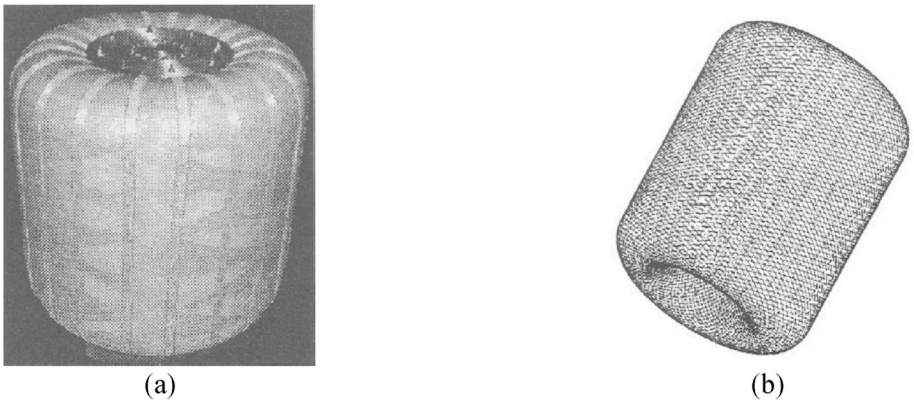

Fig. 24. a) Model created by filament winding; b) FE mesh for the analysis of toroidal structure, Harris & Kennedy [154].

membrane-best withstands tensile forces. The importance of a realistic anchoring which can reduce or even eliminate uplifting effects is also highlighted.

4.3. Deployable structures

Another popular concept for implementing ET structures is the concept of deployable structures: these are able to change their shape, and hence their size, according to the requirements. Furthermore, such structures hold strong potential for mass reduction. The deployable technology is already applied for terrestrial constructions (e.g. umbrellas, elevating machines, etc.) and also applies to space constructions (e.g. solar panels, solar sails, space antennae, etc.), since such structures can be compactly stowed during launch and yet can be functional and reconfigurable after reaching the destination [160,161]. However, only a few studies have highlighted the fact that such structures have the potential to serve as human habitats and outposts in Lunar and Martian environments. A selection of these studies is presented in this section.

Ng (2006) [162]

The folding process of a deployable structure incorporating nine integral folding hinges (IFH) is examined in this paper with the use of numerical modeling and finite element analysis (Fig. 30a). The elastic hinge of the deployable structure is a doubly slit cylindrical segment made of composite materials (laminates of AS4 Carbon PEEK) and behaves like a standard truss member when deployed (Fig. 30b). Although various configurations of IFH have already been developed, the novelty of this project is that it investigates their dynamics, which are important to the design of deployable structures. At a next stage, the validation of the numerical model is accomplished by using the experimental data from the Air Force Research Laboratory, where the deployment of the same physical deployable structure is studied using photometry technique. Finally, the designer is allowed to use the numerical model for future space structures.

Tinker et al. (2006) [163]

This paper constitutes a review on deployable structures for use in ET environments. In particular, two types of structures are presented: (a) deployable metal/composite structures, and (b) thin-film inflatable (TFI) structures. Furthermore, regarding the construction method, the research described in this paper includes: (1) near-term inflatable and deployable components fabricated on Earth and then combined with in-situ materials on a ET planetary surface, and (2) far-term concepts constructed primarily using in-situ resources. The main focus of this work is upon the nearer-term concepts, in conjunction with terrestrial and in-situ materials. Types of structures introduced in this paper include: (i) various inflatable concepts including stowed, telescoping and inflatable cylinders, (ii) contour crafting (the most popular method of construction in ET environments so far) using in-situ materials, (iii) inflatable Lunar dome combined with contour crafting either by providing support for the crafted in-situ material or by providing a pressure barrier on the inside. The importance and novelty of this project stems from the fact that it combines all the aforementioned types of structures with the in-situ material of the ET environment and also depicts an early stage of the most recent concepts for construction in ET environments (e.g., 3D-printing by using regolith as structural material).

Woodruff and Filipov (2018) [164]

This work is inspired by origami structures and presents a finite

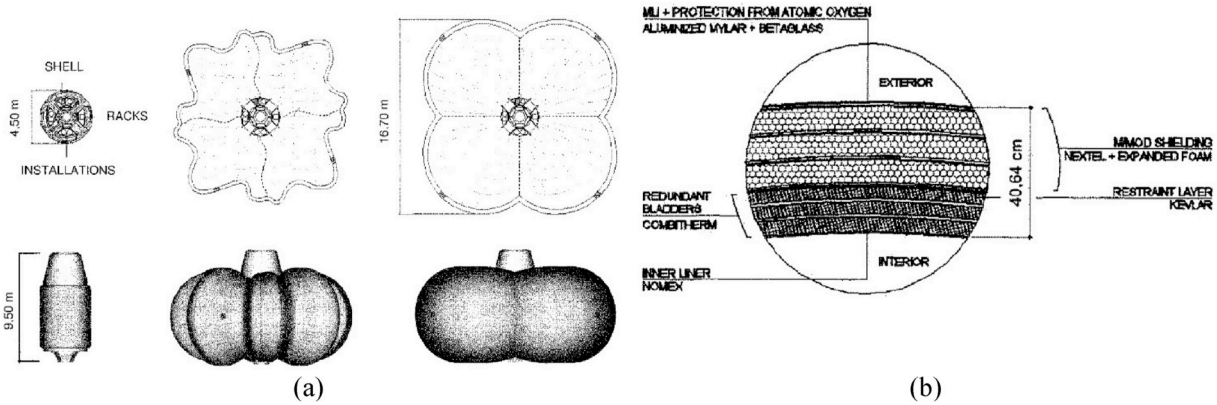

(a) (b)

Fig. 25. a) Inflation phases of the “Astrophytum”, b) the five main layers of the shell, Borin & Fiscelli [156].

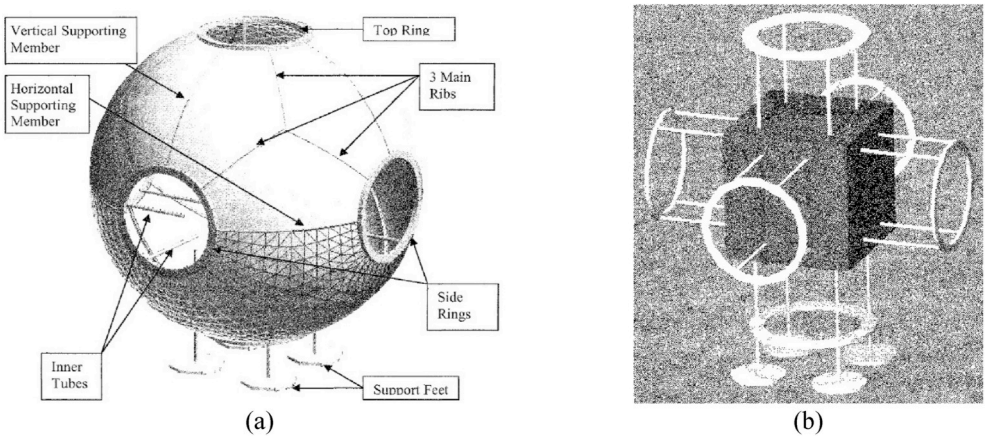

Fig. 26. a) Overview of an open single unit; b) Core, extended supports and mating ring units without membrane, Criswell & Carlson [157].

element analysis/implementation of thin sheets made of Mylar which are folded in a curve creased origami configuration. The computational model makes use of shell elements to capture the deformations and rotational hinges in order to simulate the crease line. Four alternative methods for actuating/folding the crease are introduced and corroborated through empirical solutions for a curved crease structure, as shown in Fig. 31. Each of the four actuation methods comes with its own functional advantages and disadvantages, which must be considered when deciding how to model a curved crease structure. It is shown that, for all methods, bending energy is lower at the edges of the sheet, with distributed bending energy increasing towards the inner radius of the curved crease system. In-plane energy is smaller compared to the out-of-plane bending. Stretching and shearing accounted for 5% of the total energy when out-of-plane forces were used to fold the system.

4.4. 3D-printed ET structures

With the advancement of technology, Additive Manufacturing (AM) technology is receiving increasing attention due to its potential to produce various geometrically complex structures. Some of these modern technologies rely on an agglomeration process of inert materials (e.g., sand), through a special binding fluid. This ability is of great interest for the space exploration community due to its potential application within an ISRU framework towards the construction of habitats and outposts in extreme environments. More specifically, 3D printing constitutes a pioneering and promising process that combines many disciplines (robotics, networks, sensing, etc.) and aspires to utilize indigenous soil material (regolith) to develop individual structural elements or modules on site. Aiming at the development of fundamental technologies necessary to manufacture extraterrestrial habitats with indigenous materials, NASA showed great interest in 3D-printing techniques [165]. The most effective AM fabrication method in extraterrestrial environments is based on sintering the local materials. Sintering is the heating of a porous material up to a particular temperature (below the melting point) which allows its particles to bond together with a concurrent decreasing of their porosity [166]. It has been stated that AM methods, including Fused Deposition Modeling (FDM) and

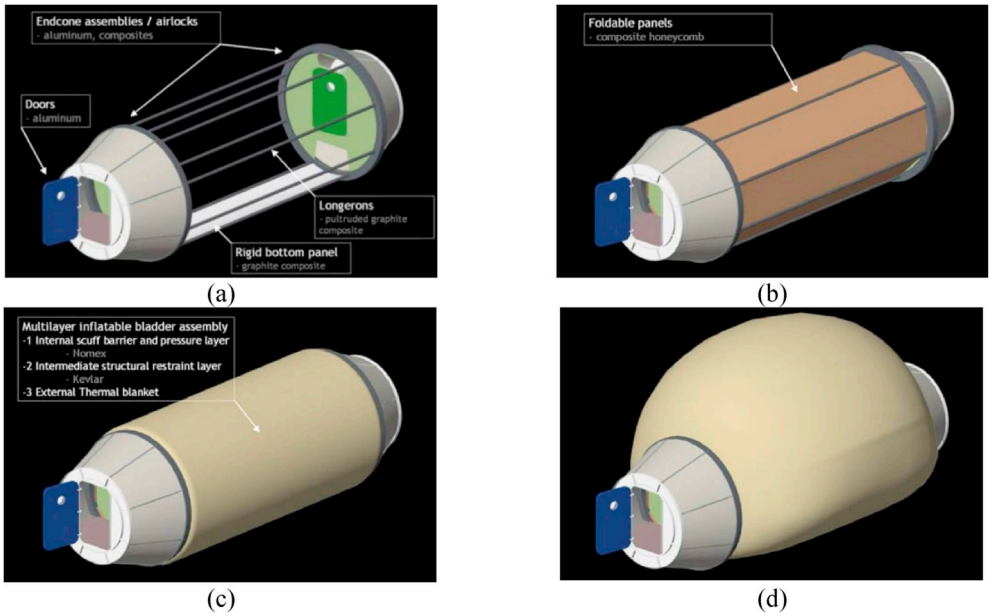

Fig. 27. a) Rigid frame of SEIM; b) modular panels in the transit configuration; c) rigid frame and folded bladder in the transit configuration; d) rigid frame and inflated bladder in the deployed configuration, Adams & Petrov [158].

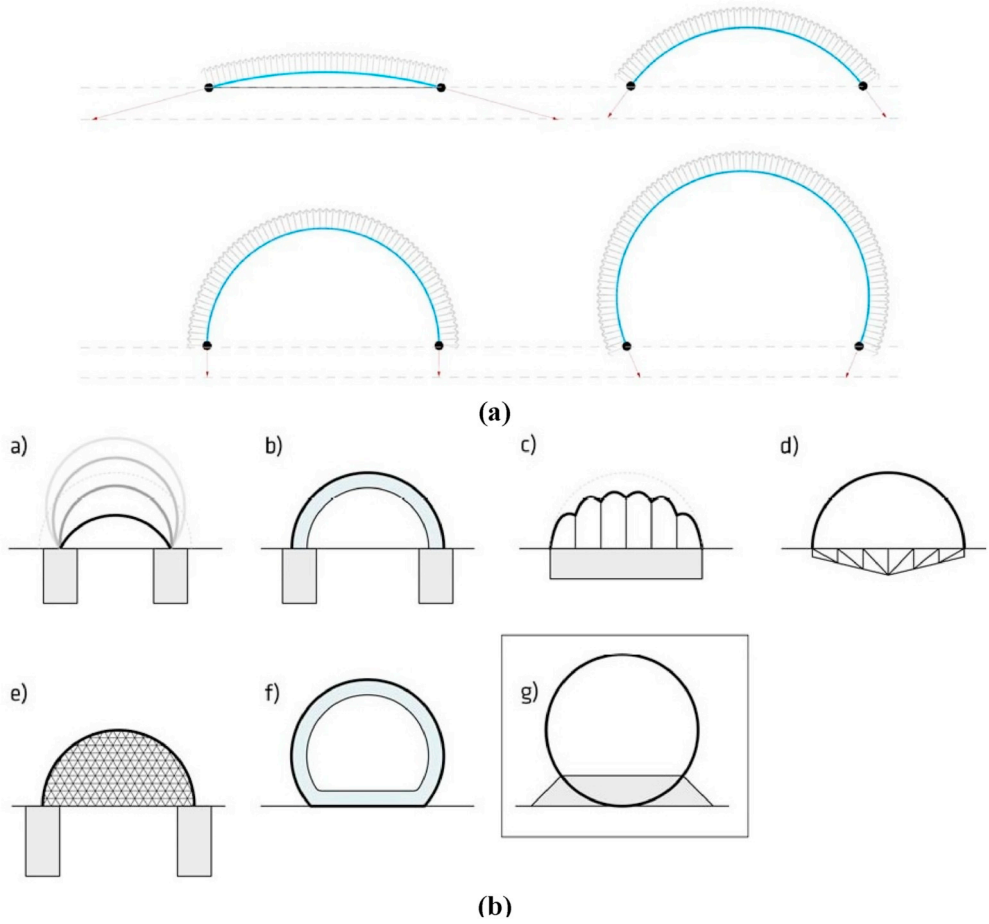

Fig. 28. i) Reaction forces of various arc configurations; ii) overview of the investigated structural solutions, Brandt-Olsen et al. [159].

Selective Laser (or Solar or Microwave) Sintering, can be used as potential fabrication methods for Lunar construction [167]. In particular, Mueller et al. [167] present an overview on the state-of-the-art in Automated Additive Construction (AAC) methods using ISRU, where: (a) the general lack of knowledge in the existing AM technologies is highlighted, (b) opportunities for investments are investigated, and (c) potential technology demonstration missions for Lunar and Martian environments is proposed.

Regarding the Laser sintering method, there are relatively few works in this field [168]; Fateri and Gebhardt, 2015; [169,170]. Regardless of the residual and thermal transient stresses produced during the sintering of raw regolith, the corresponding experiments confirmed

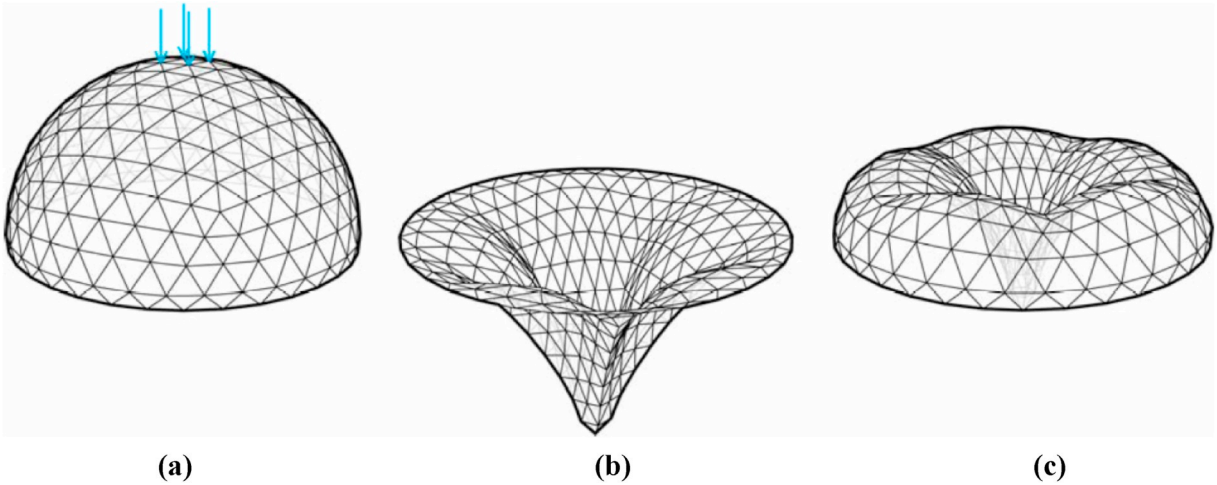

Fig. 29. Pressure simulation via Kangaroo: a) undeformed shape indicating where the point loads are applied; b) deformed shape with constant pressure; c) deformed shape with volume-aware pressure, Brandt-Olsen et al. [159].

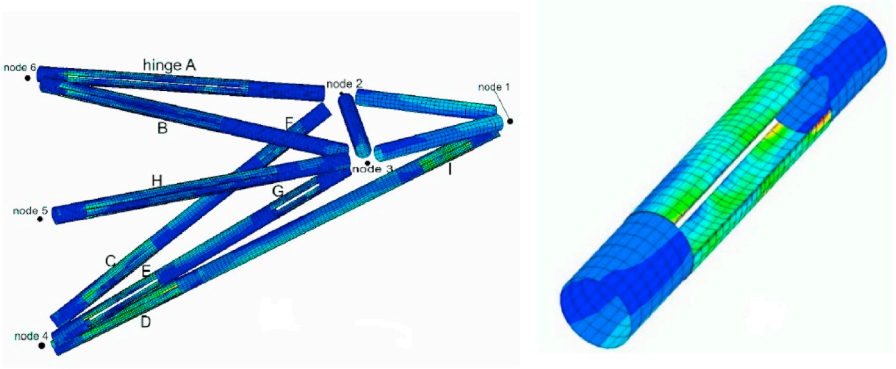

Fig. 30. a) Finite element model b) Integral folding hinge, Ng [162].

that the samples were successfully sintered and formed into the expected parts at a high level of geometrical accuracy. Such experiments included e.g. a 10 × 25 mm cylinder made of JSC-1AC [168], a 30 × 30 mm net-shape object of JSC-1A (Fateri and Gebhardt, 2015), and a 20 × 20 × 5 mm cubic sample made of JSC-MARS-1A [169]. However, direct sintering alone is not considered as the optimum fabrication method for a large-scale ET construction, since: i) the total amount of energy required would be extremely high (e.g., requiring a nuclear power source), and ii) only a small volume of material can be thermally treated at a time, necessitating longer printing times for wider areas [171].

On the other hand, due to the unlimited supply of solar energy, solar sintering could potentially be a suitable fabrication technique, readily available on the Lunar surface. Various researchers have investigated the potential of producing Lunar glass composite structures [172], Lunar concrete [173], surface stabilization [174], and Lunar brick [175] using solar energy. Despite the advantages of solar-concentrated sintering methods, there are certain shortcomings. One serious disadvantage of these methods is that the system requires additional complexity in order to clean the lenses and mirrors of Lunar dust and also to maintain positioning controls to focus on the desired focal spot location relative to the movement of the sun and the solar concentrator [176]. Furthermore, the optical properties of Lunar regolith may affect the effectiveness of the concentrator. For example, the darker mare regions would absorb more light, so it would be heated more efficiently by the solar concentrator than highlands regolith, all other properties remaining the same [177]. Also, the solar concentrator would not be an option at certain potential landing-sites where the surface is not directly exposed to sunlight.

The most promising technique for regolith sintering is by means of microwaves, where the depth penetration of the heat during the sintering is better than both solar and laser sintering (melting of Lunar simulant up to a 13.4 mm depth for 2.45 GHz microwaves, [178]. Until now, most studies on microwave sintering, whether on original regolith or Lunar simulants, have been conducted at 2.45 GHz microwave frequency. Microwave energy can be used for fabricating wider areas, e.g. pavement and/or spacecraft launch and landing pads etc., and the importance of microwave energy applied on Lunar regolith has been highlighted by Taylor and Meek [179] and Taylor et al. [180]. Several researchers [167,181–184] have further investigated a microwave sintering technique utilizing a Lunar simulant as a potential fabrication method.

Various researchers believe robotics combined with AM technologies have reached an adequate level for terrestrial applications and thus have huge potential to become the catalyst for space colonization [171]. Two significant works -including laboratory experiments-on the construction processes of the prospective extraterrestrial structures by means of AM are presented below.

Khoshnevis & Zhang (2012) [181]

This project presents the Contour Crafting (CC) technology, which is

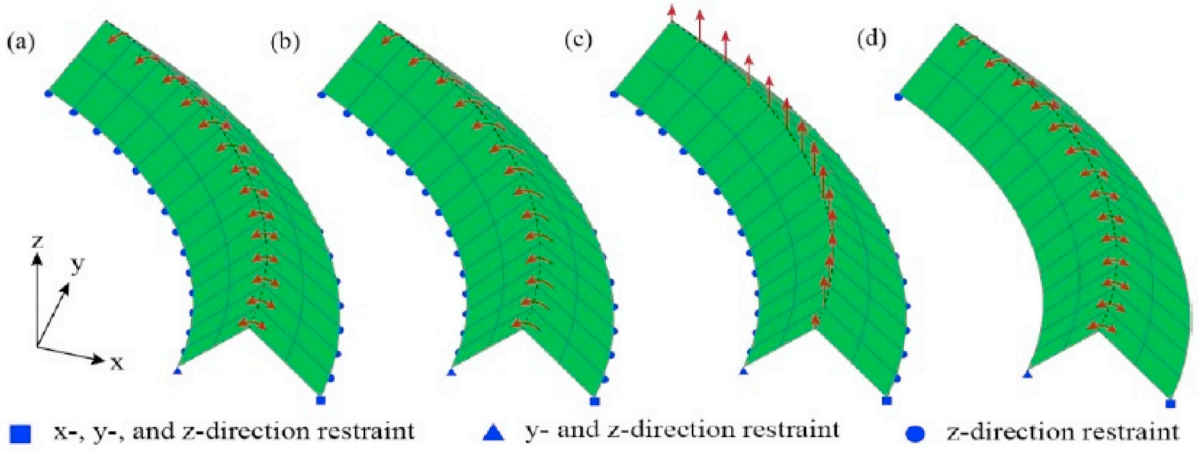

Fig. 31. Different boundary conditions applied on the structure to simulate folding: a) Applied Rotations, b) applied moments, c) applied force, and d) applied rotations and reduced z-restraints, Woodruff and Filipov [164].

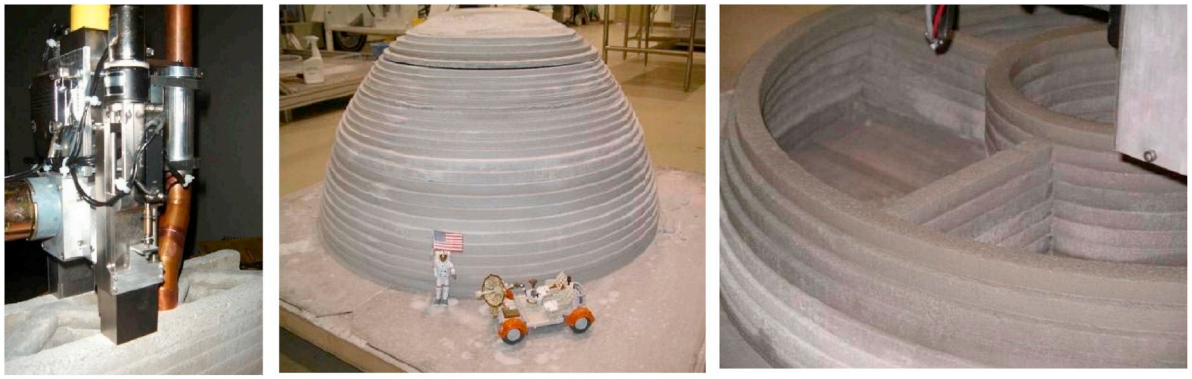

Fig. 32. Contour crafting: a) Co-extrusion CC nozzle building walls with corrugated fill; b) & c) Dome structures built by means of contour crafting, [181].

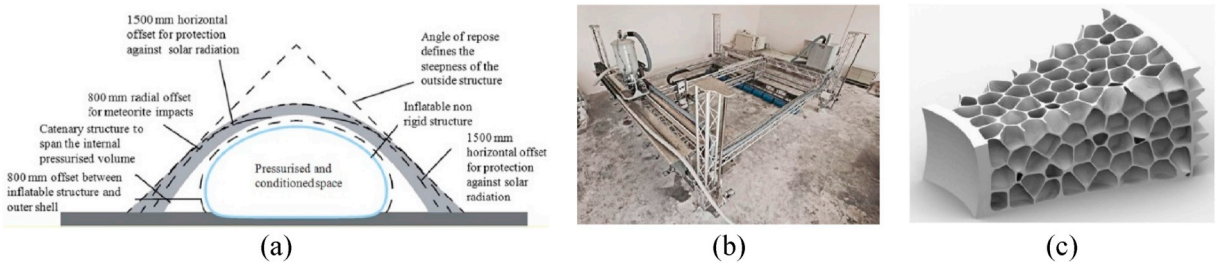

Fig. 33. a) Schematic of the outpost structure; b) D-shape printer; c) exemplar structural element, Cesaretti et al. [185].

a large-scale AM process, in conjunction with in-situ materials, customized for fast and reliable Lunar infrastructure development (Fig. 32) in combination with sulfur concrete and regolith sintering. Various experiments have demonstrated the applicability of the aforementioned procedure, where such mixtures have proven feasible in the lab setup prototype systems. In particular, these experiments were conducted using sulfur-based concrete, and sintered Lunar regolith simulant (JSC-1A) mixed with steel or copper powder, or even without any additives. The results showed that CC technology can indeed be combined with such materials. The compressive strength of sintered plain regolith and mixture could reach 55.16 MPa, which is strong enough for building ET structures such as landing pads, blast walls and hangers. Two main uses of the sintered regolith are proposed in this project: (a) Regolith sintering can be carried out on the construction site for the production of the main construction material. (b) The regolith can be sintered into regular shapes such as blocks, voussoirs and bricks; then a layer of regolith bricks can be combined with sulfur concrete extrusion, a second layer of regolith bricks may be paved above the first, with a compression force applied; this combination will enhance the strength of the extraterrestrial constructions. According to a possible CC process variation, the regolith mixture will be delivered to the construction site, kept in the confines of three trowels of the nozzle. Then, the mixture will be exposed to sintering heat for a certain time while the delivery nozzle will slowly move.

Cesaretti et al., (2014) [185]

This project assesses a 3D-printing technology concept for building Lunar habitats by incorporating indigenous soil material. The authors state that a 3D-printed “shielding” structure is needed in order to protect the habitable pressurized modules from ET natural hazards (radiation, temperature fluctuation, meteorite impacts), as shown in Fig. 33a. A patented 3D-printing technology named “D-shape” is presented (Fig. 33b). For the needs of the D-shape technology, a novel Lunar regolith simulant (DNA-1) that resembles the characteristics of JSC-1A was developed. The researchers performed various tests (including under vacuum conditions) to demonstrate the occurrence of a reticulation reaction with the simulant. Tests in vacuum showed that problems such as freezing or evaporation of the bind liquid can be avoided if a proper injection method is used. The specifications of the main requirements of a Lunar outpost, along with the development of a preliminary design of the habitat, were performed by Foster and Partners (F + P). Based on the preliminary design, a section of the outpost wall was selected and manufactured at full-scale using the D-shape printer and regolith simulant. Test pieces were also manufactured and their mechanical properties were assessed. The structural design focused on the minimization of the ratio of consolidated material over rough regolith. The result of such a trade-off is provided by a particular topology named closed foam (Fig. 33c).

Table 11 summarizes the main characteristics of each ET structural concept presented in section 4, so as to provide a visual overview and comparison of all methods compiled herein. The fields include the structural type, the input or loading, the type of analysis or approach, and the material. The acronyms used are explained at the bottom of the table.

Table 11
Summary of ET structural concepts presented in section 4.

Reference	Structural type	Input/Loading	Analysis/approach	Structural material
Benaroya & Ettouney (1992a) [129]	Flat Truss	GL (regolith shield, structural elements); IP	LS	N/A
Ettouney et al. (1992) [131]	Cabled	N/A	N/A	N/A
Benaroya & Ettouney (1992b) [130]	Steel	GL (regolith shield, structural elements); IP	LS, LD	Steel
Nowak & Sadeh (1992) [147]	Inflatable	GL (regolith shield, structural elements); IP	LS, FEA	Kevlar 49
Benaroya (1993) [132]	Tension cable or "Tensegrity"	GL (regolith shield, structural elements); IP	N/A	N/A
Sadeh & Criswell (1993) [149]	Inflatable	GL (regolith shield, structural elements); IP	LS, FEA	Kevlar 49
Sadeh & Criswell (1994) [149]	Inflatable	GL (regolith shield, structural elements); IP	LS, FEA	Kevlar 49
Jolly et al. (1994) [133]	Flat Truss	GL (regolith shield, structural elements); IP	LS	Composite material with a density of 1.523 kg/m^3 (assumption)
Malla et al. (1995) [134]	Flat Truss	GL (regolith shield, structural elements); IP	LS, LD, FEA	Aluminum
Abarbanel et al. (1996) [150]	Inflatable	GL (regolith shield); IP	LS, FEA	Isotropic Kevlar 49
Cadogan et al. (1999) [151]	Inflatable	N/A	N/A	Kevlar
Kennedy (1999) [152]	Inflatable	N/A	AA	Kevlar
Aulesa et al. (2000) [6]	Dome	GL (regolith shield, structural elements); IP	LS	Cast basalt
Bateman et al. (2000) [153]	Inflatable	GL, IP	LS, FEA	Kevlar
Kennedy (2000) [154]	Inflatable	Arbitrary Axial loading applied at each fiber	LS, FEA	Kevlar, Bias fibers at an angle of 67 deg
Jenkins and Tampi (2000) [155]	Inflatable	LV	LD	Mylar polyester
Borin & Fiscelli (2004) [156]	Inflatable	N/A	AA	Five layers made of mainly Kevlar (Fig. 13b)
Criswell & Carlson (2004) [157]	Inflatable	IP	LS	Kevlar
Adams & Petrov (2006) [158]	Inflatable	N/A	AA	Shell made by Kevlar and core made by carbon fiber
Ng (2006) [162]	Deployable	Arbitrarily applied external load (offload of 90 N) and gravity load	LD, FEA	laminates of AS4 Carbon PEEK
Tinker et al. (2006) [163]	Inflatable & Deployable	N/A	N/A	Varies (review paper)
Benaroya (2006) [135]	Arch	GL (regolith shield, structural elements); IP	FEA	High strength aluminum
Ruess et al. (2006) [136]	Arch	GL (regolith shield, structural elements); IP	FEA	High strength aluminum
Malla & Chaudhuri (2006) [137]	Truss & inflatable	GL (regolith shield, structural elements); IP	FEA	Frame of aluminum, membrane of Kevlar
Meyers & Toutanji (2007) [138]	Hemispherical Dome	GL (regolith shield, structural elements); IP	LS, TA	Waterless regolith concrete and glass fibers
Malla & Chaudhuri (2008) [139]	Truss & inflatable	GL (regolith shield, structural elements); IP; IL	NLD	Frame of aluminum, membrane of Kevlar
Faierson et al. (2010) [141]	Voussoir Dome	GL (dome)	LS	Regolith combined with aluminum powder
Khoshnevis & Zhang (2012) [181]	3D-printed	N/A	N/A	Regolith & sulfur concrete
Malla & Gionet (2013) [140]	Truss & inflatable	GL (regolith shield, structural elements); IP; IL	NLD	Frame of aluminum, membrane of Kevlar
Cesarreti et al. (2014)[185]	3D-printed	N/A GL (regolith shield)	FEA	Regolith simulant (DNA)
Mottaghi & Benaroya (2015a) [142]	Igloo-shaped	GL, IP	TA	Magnesium alloy
Mottaghi & Benaroya (2015b) [143]	Igloo-shaped	GL, IP, SL	FEA, LS, MA, RVA	Magnesium alloy
Brandt-Olsen et al. (2018) [159]	Inflatable	GL, IP	FEA	Kevlar cable and ETFE membrane
Woodruff & Filipov (2018) [164]	Deployable	N/A	FEA and empirical methods	Mylar

GL: Gravity Loading, IP: Internal pressure, IL: Impact Loading, SL: Seismic Loading, TF: Temperature Fluctuation, SR: Solar Radiation, LS: Linear Static analysis, LD: Linear Dynamic analysis, NLD: NonLinear Dynamic analysis, LV: Laser vibrometer, FEA: Finite Element Analysis, TA: Thermal Analysis, AA: Architectural Approach, RVA: Random Vibrations Analysis, MA: Modal Analysis.

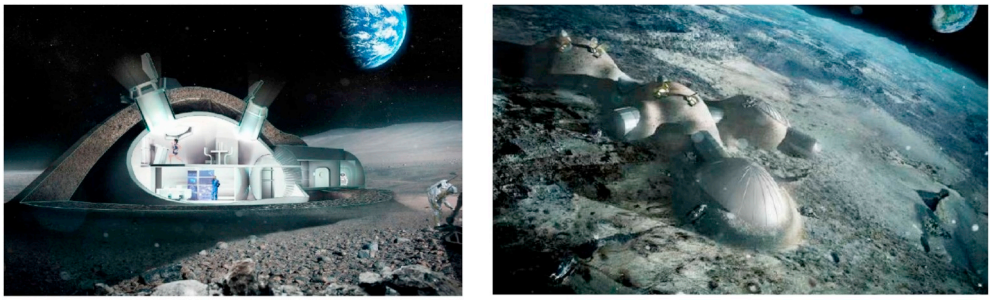

Fig. 34. a) Section of a Lunar module; b) View of a Lunar outpost, De Kestelier et al. [190].

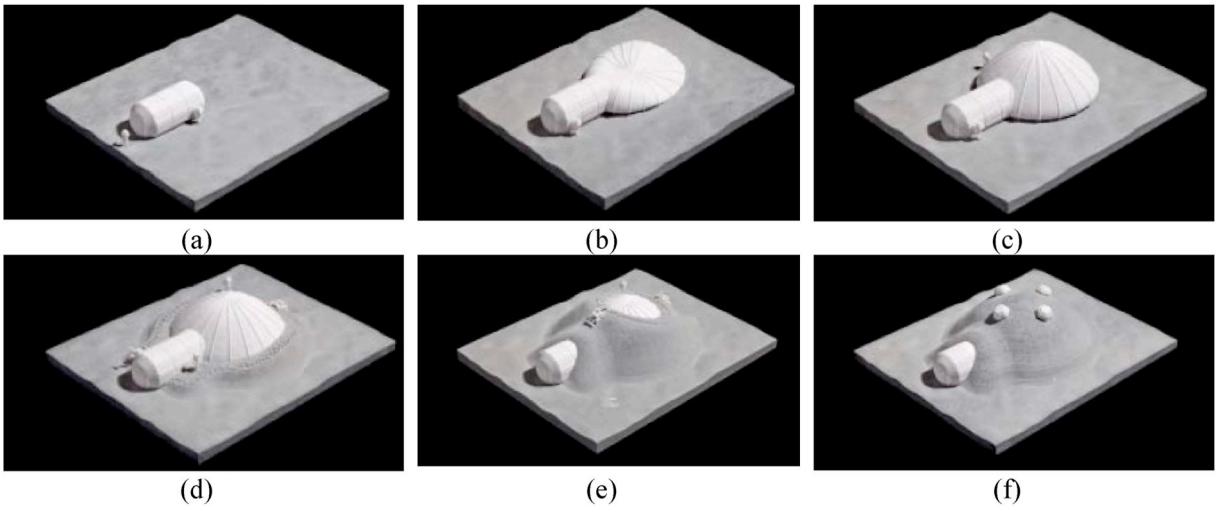

Fig. 35. Progressive construction of a Lunar module, De Kestelier et al. [190].

5. Human-centered concepts for lunar/martian outposts

The previous section focused on individual structures, and the techniques and materials that could be used to design and construct them from a civil/structural/material engineering point of view. In this section, the focus shifts to a more holistic conceptualization of a human habitat by employing a combination of large-scale additive manufacturing, ISRU, robotics, inflatable structures, or even modular assembly in low-Earth orbit. It is evident that the project planning and management requires many engineering disciplines working towards a common target. Furthermore, the requirement for the efficient command and control of the robots needed to build, operate and service different components of the habitat can become critical [186].

One of the most radical ideas for the construction of a Lunar habitation base is the Modular Assembly in Low-Earth Orbit (MALEO) strategy [187]. According to this, the components of the Lunar base will be brought up to low-Earth orbit by the space transportation system and assembled there in order to construct the final form of the Lunar base. After the construction of the Lunar base, specially designed propulsion systems will be used for its safe transportation to the Moon. The MALEO systems for deploying a Lunar habitation base (LHB-1) must be highly reliable and consist of: i) a structurally-strengthened Lunar habitation base, ii) a chemical/electric modular orbital transfer vehicle (MOTV), and iii) a Lunar landing system (LLS).

An Initial Manned Lunar Outpost (IMLO) concept is proposed by Bell et al. [188]. From a structural point of view, the modules of the outpost are placed under the Regolith Support Structure (RSS), which provides a safe environment and radiation protection for the entire base. The overhead structure was chosen over simply burying the modules for reasons of easy access to the surface (exterior of the modules) and in order to provide shelter for the vehicles and mechanical equipment. Furthermore, since certain terrestrial regions such as areas in Antarctica resemble the Lunar/Martian environment and terrain more than any other place on Earth, Bell and Trotti [189] propose the construction of a facility for research there, in order to best simulate real extraterrestrial conditions.

The pioneering work of De Kestelier et al. (2015) focuses on a holistic approach to the design of a Lunar outpost (Fig. 34) and emphasizes two main aspects. Firstly, the examination of the technical feasibility of 3D printing, incorporating Lunar regolith where the chemical and physical characteristics of Lunar regolith and terrestrial regolith simulant will be examined and assessed to check if it is a viable construction material for large-scale 3D printing. Secondly, the project focuses on how 3D-printed structures could be used as shielding and how this could be integrated within the overall design of a Lunar outpost. Furthermore, this paper investigates various methods towards the increase of the protective capacity (using regolith shielding) of 3D-printed structures (Fig. 35), along with the integration of such structures within the overall design of a Lunar outpost. More specifically, the current design incorporates an assembly of three inflatable volumes (Fig. 34b), interconnected with ready-to-use cylindrical elements that also form air locks to the outside environment. The inflatable part will have a height of 5 m in order to span two levels (storeys) in height. Furthermore, the authors propose a dome-shaped shell constructed from 3D printed regolith -making use of D-shape 3D printing technology-that will act as shielding for the inflatable part. Since the D-printing process uses its own powder as support structure, the dome would need to be hollowed out after being printed. This procedure would need excavations, which would be tremendously energy-consuming and risky for the structural health. To this end, the authors

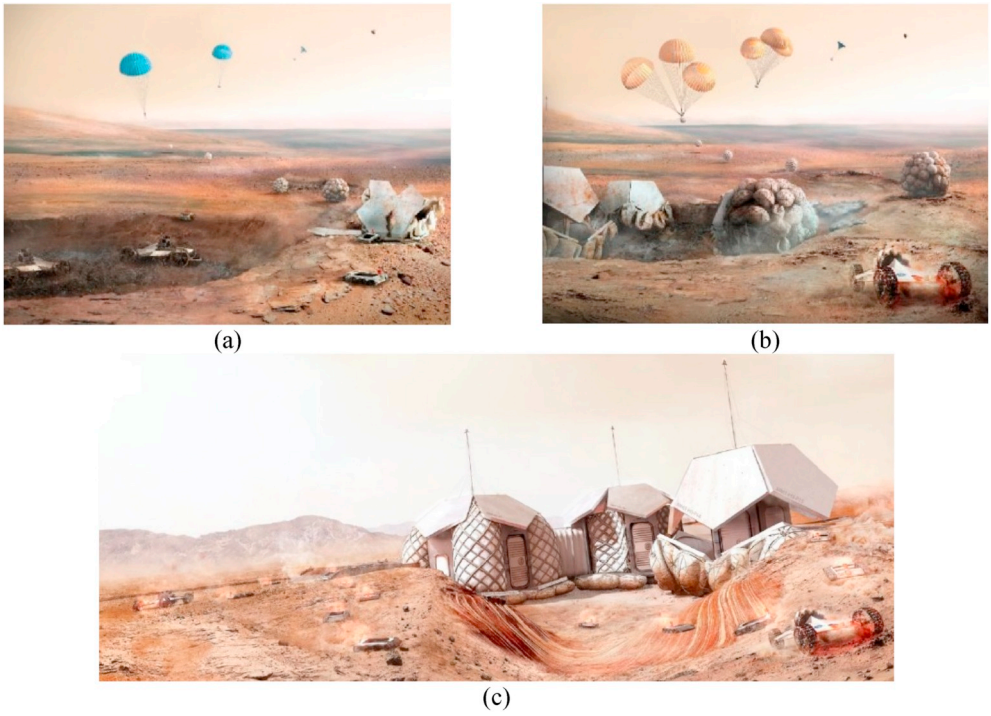

Fig. 36. a) Entry, descent and landing (EDL) of multi-robots for site preparation; b) EDL and navigation of the habitat units; c) deployment of modules (opening, inflation and connection), Wilkinson et al. [191].

propose the creation of an additional inflatable structure that would serve as a support on which the dome can be constructed (Fig. 35). A closed-wall foamed system was chosen as the internal structure within the regolith shield (Fig. 33c).

Wilkinson et al. [191] present the construction process for an inhabitable outpost on the Martian surface. They propose an autonomous multi-robot swarm approach (Fig. 36) for the construction (through large-scale AM techniques) of protective shielding (consisting of layers

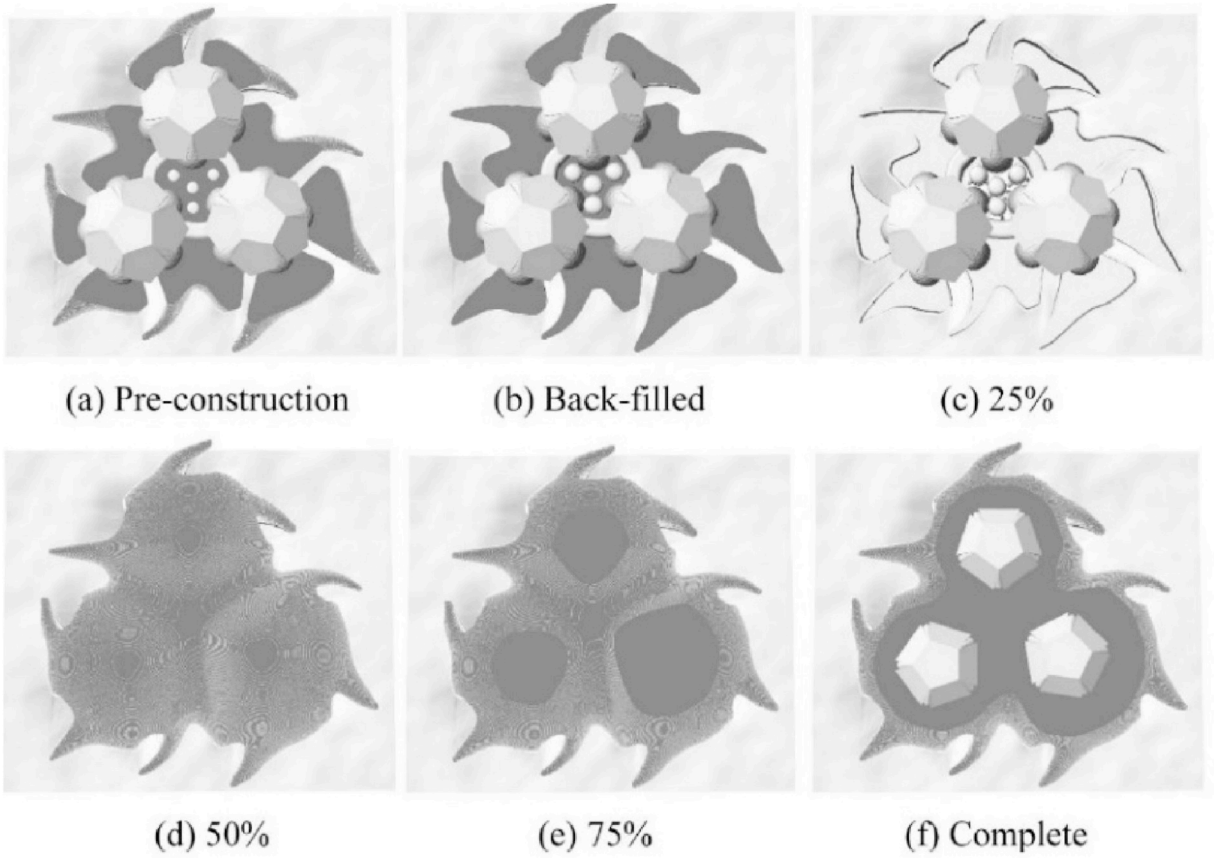

Fig. 37. View progress of regolith construction, Wilkinson et al. [191].

of sintered regolith) over an inflatable pressurized module (Fig. 37). The sintering of regolith will be performed with the use of microwave power. The main design idea of this work is that a configuration of multiple simpler units working in parallel -instead of a simple complex unit-can lead to higher probability of success, since the risk is physically distributed among the simpler sub-tasks.

6. Discussion

This review paper presents a compilation of distilled information relevant to the conceptualization and design of the first ET structures from a civil engineering perspective, considering other relevant aspects. The range of information spans a very wide spectrum, from Lunar and Martian regolith properties and ET ground motions caused by moonquakes and meteor impacts to structural analysis and design. To the best of their knowledge, the authors try to compile the most important and prevalent ideas across these fields, remaining aware that a truly exhaustive compilation would be close to impossible. Instead, we try to bring together for the first time some of the different disciplines we believe are key to designing ET structures, in the hope that this may facilitate future multidisciplinary communication and collaboration.

In terms of shear strength, and despite the large variability in measurement results, Lunar and Martian regolith samples do not exhibit high values of cohesion (generally less than 6 kPa). However, they can reach up to (and even more than) 40°of internal friction angle, which could prove useful for excavations or for transferring compressive loads from the superstructure. Furthermore, aside from their high silicate content (>42%), they combine iron and aluminum oxides, which together can reach more than 25% for Martian regolith and even more than 30% for Lunar regolith. This considerable iron and aluminum oxide content could be potentially invaluable for forming strong and relatively ductile structural materials if treated properly.

Consideration of the four main sources of ground motion recorded on the moon –shallow, deep and thermal moonquakes and meteor impacts-in terms of occurrence, amplitude, location, repeatability etc., shows that -in all probability-only shallow moonquakes and impacts have the potential to constitute hazards for potential ET structures. Although recorded amplitudes are small due to large distances, shallow moonquakes up to m_b 5.5 or more have been observed; and while the most frequent meteor impactors may weigh a fraction of a kg, there is potential for impactors weighing several tons. However, the observation period of these phenomena is extremely short (only about 8 years) and unfortunately it ended in 1977. This means we have missed out on precious data over the past 43 years, which could have improved our knowledge on occurrence rates and other topics affecting probabilistic hazard assessment. At the same time, available recordings come from unusually long distances (over 500 km and often closer to 1000 km). This will render the task of extrapolating to short distances very challenging, whether it is eventually performed through empirical relations or simulations.

Table 11 summarizes in a concise and illustrative way the structural concepts and approaches for designing potential ET structures. The first challenges identified by the pioneering engineers were: (a) protection from extreme radiation; (b) higher internal (to external) pressures, and (c) appropriate structural materials. Interestingly, in each decade there took place a significant change in the engineering approach. During the 1990s and almost simultaneously, two leading groups of researchers envisioned future Lunar structures either as strong yet lightweight inflatable modules using mainly Kevlar, or as flat truss structures supporting a regolith shield. Regolith shielding was deemed necessary to protect against radiation, and in some cases against extreme temperature fluctuations, while Kevlar for the protection against direct meteorite impacts. Only after the turning of the century did engineers start using arch-type structures or domes, utilizing mainly high-strength aluminum (for the arch trusses) and indigenous materials (regolith), and in many cases combining them with inflatable structures. However, it was only during the current decade of the 2010s that, following technological advancements, researchers first considered the construction method as well, and thus envisioned the first 3D-printed structures using regolith in an ISRU framework.

In terms of loading considerations, the most usual combination was gravitational loads including the weight of the structural members and the regolith shielding, together with high internal pressures, which dominate on the Lunar surface due to microgravity and the lack of atmospheric external pressures. Therefore, the potential habitable structures mainly needed to withstand tension, in addition to not occupying a lot of space during their transportation; hence, inflatable structures were the most oft-proposed potential Lunar structures. Furthermore, only a few sporadic studies took into account dynamic loading such as meteorite impacts, and even fewer considered loading from the seismic ground motions on the Lunar surface (moonquakes).

Today, we believe there is a strong and clear need for a fresh civil engineering vision, following upon the novel architectural propositions of De Kastellier et al. [190] and Wilkinson et al. [191]. More specifically, there is a need for regolith-based ET structures that will exhibit resilience against natural hazards, also considering dynamic loading in the form of seismic ground motions and impacts, and constructed using large-scale additive manufacturing, interlocking regolith bricks, or other compaction/sintering techniques. These long-span regolith-based structures could act as shielding structures to protect the future inflatable, habitable modules as well as valuable assets such as robots, energy tanks, etc. Additionally, we believe a multiphysics framework should be adopted, as it would ideally couple thermal with static and dynamic (linear and nonlinear) analyses, thus resulting in more realistic simulations and scenarios; such an approach should now become feasible, given that computational power has increased significantly compared to previous decades. Finally, for validating the numerical scenarios including structural or geotechnical models (considering foundation, excavations/anchoring/drilling), we believe that further experimental work conducted using small-scale microgravity simulations via centrifuge testing could shed more light onto the real dynamic behavior of regolith-based (or inflatable) structures in low gravity conditions incorporating different soil-structure interaction (SSI) considerations.

Declaration of competing interests

The authors declare that they have no known competing financial interests or personal relationships that could have appeared to influence the work reported in this paper.

Acknowledgements

This review paper is part of the project entitled “Designing for the Future: Optimising the structural form of regolith-based monolithic vaults in low-gravity conditions” supported by the Engineering and Physical Sciences Research Council (EPSRC), UK (Scheme: New Investigator Award), led by the University of Greenwich. EPSRC Reference: EP/S036393/1. We are grateful to two anonymous reviewers for their patient scrutiny of the manuscript and suggestion of additional literature sources.

References

[1] M. Trial, Some effects of declining US university civil engineering enrollments on the space enterprise, Space (2000) 308–311 2000.
[2] H. Benaroya, L. Bernold, Engineering of lunar bases, Acta Astronaut. 62 (4–5) (2008) 277–299.
[3] A.M. Jablonski, D. Showalter, An introduction to AIT requirements for lunar systems and structures, Earth and Space 2016: Engineering for Extreme Environments, American Society of Civil Engineers, Reston, VA, 2016, pp. 546–559.
[4] H. Benaroya, Lunar habitats: a brief overview of issues and concepts, Reach. Out. 7

(2017) 14–33.
[5] D.G. Schrunk, B.L. Sharpe, B.L. Cooper, M. Thangavelu, The moon: resources, future development, and settlement, second ed., in: David G. Schrunk, Burton L. Sharpe, L. Bonnie (Eds.), Cooper and Madhu Thangavelu, Published by Springer-Praxis, New York, NY USA, 978-0-387-36055-3, 20082008.
[6] V. Aulesa, F. Ruiz, I. Casanova, Structural requirements for the construction of shelters on planetary surfaces, Space 2000 (2000) 403–409.
[7] A.M. Jablonski, K.A. Ogden, Technical requirements for lunar structures, J. Aero. Eng. 21 (2) (2008) 72–90.
[8] T.A. Parnell, J.W. Watts Jr., T.W. Armstrong, Radiation effects and protection for moon and mars missions, Space (1998) 232–244 1998.
[9] G. Reitz, T. Berger, D. Matthiae, Radiation exposure in the moon environment, Planet. Space Sci. 74 (1) (2012) 78–83.
[10] Ph Lognonné, M. Le Feuvre, C.L. Johnson, R.C. Weber, Moon meteoritic seismic hum: steady state prediction, J. Geophys. Res. B 114 (E12003) (2009).
[11] C. Hirt, W.E. Featherstone, A 1.5km-resolution gravity field model of the Moon, Earth Planet Sci. Lett. 329–330 (2012) 22–30.
[12] N. Kalapodis, G. Kampas, O.-J. Ktenidou, Revisiting the fundamental structural dynamic systems: the effect of low gravity, Archive of Archive of Applied Mechanics 10 (2019) 1861–1884.
[13] N. Kalapodis, G. Kampas, J. Webb, O.-J. Ktenidou, The effect of self-weight on free-standing blocks, 2nd International Conference on Natural Hazards & Infrastructures (ICONHIC 2019), 2019.
[14] G. Petrov, J. Oschendorf, Building on mars, Civil Engineering, American Society of Civil Engineers 75 (10) (2005) 46–53.
[15] B.A. Schock, C.L. Caleb Hing, A civil engineering approach to development of the built martian environment, Earth Space (2015) 313–327 2014.
[16] A. Genova, S. Goossens, F.G. Lemoine, E. Mazarico, G.A. Neumann, D.E. Smith, M.T. Zuber, Seasonal and static gravity field of Mars from MGS, Mars Odyssey and MRO radio science, Icarus 272 (2016) 228–245.
[17] B.M. Jakosky, R.J. Phillips, Mars' volatile and climate history, Nature 412 (6843) (2001) 237–244.
[18] M. Gurwell, E. Bergin, G. Melnick, V. Tolls, Mars surface and atmospheric temperature during the 2001 global dust storm, Icarus 175 (1) (2005) 23–31.
[19] R. Wilson, The martian atmosphere during the viking mission, I infrared measurements of atmospheric temperatures revisited, Icarus 145 (2) (2000) 555–579.
[20] M. Thomas, N.L. Wong, Regolith research in Australia, Aust. J. Earth Sci. 64 (8) (2017) 983–985.
[21] Grant H. Heiken, David T. Vaniman, Bevan M. French, Lunar Sourcebook: A User's Guide to the Moon, Cambridge University Press, 1991, p. 286.
[22] P. Morgan, M. Grott, B. Knapmeyer-Endrun, M. Golombek, P. Delage, P. Lognonné, S. Kedar, A pre-landing assessment of regolith properties at the InSight landing site, Space Sci. Rev. 214 (6) (2018).
[23] E.N. Slyuta, Physical and mechanical properties of the Lunar soil (a review), Sol. Syst. Res. 48 (5) (2014) 330–353.
[24] A.K. Leonovich, V.V. Gromov, A.V. Rybakov, V.K. Petrov, P.S. Pavlov, I.I. Cherkasov, Research of Lunar soil mechanical properties by “Lunokhod_1” self_propelled apparatus, in: A.P. Vinogradov (Ed.), Peredvizhnaya Laboratoriya Na Lune “Lunokhod_1” (“Lunokhod_1”: Movable Laboratory on the Moon), Nauka, Moscow, 1971, pp. 78–88.
[25] A.K. Leonovich, V.V. Gromov, A.D. Dmitriev, V.A. Lozhkin, P.S. Pavlov, A.V. Rybakov, Physical and mechanical properties of Lunar soil sample in nitrogen medium: research results, in: A.P. Vinogradov (Ed.), Lunnyi Grunt Iz Morya Izobiliya (Lunar Soil from Mare Fecunditatis), Nauka, Moscow, 1974, pp. 563–570.
[26] W.D. Carrier III, J.K. Mitchell, A. Mahmood, The relative density of Lunar soil, Proc. 4th Lunar Sci. Conf. (1973) 2403–2411.
[27] W.N. Houston, J.K. Mitchell, W.D. Carrier III, Lunar soil density and porosity, Proc. 5th Lunar and Planet. Sci. Conf., Houston, 1974, 1974, pp. 2361–2364.
[28] W.D. Carrier III, G.R. Olhoeft, W. Mendell, Physical properties of the Lunar surface, in: G. Heiken, D. Vaniman, B.M. French (Eds.), Lunar Sourcebook, Cambridge Univ. Press, Cambridge, 1991, pp. 475–594.
[29] E.F. Nordmeyer, Lunar Surface Mechanical Properties Derived from Track Left by Nine Meter Boulder, NASA, 1967 MSC Internal Note No. 67-TH-1.
[30] L.D. Jaffe, Surface structure and mechanical properties of the Lunar maria, J. Geophys. Res. B 72 (1967) 1727–1731.
[31] R.F. Scott, F.I. Roberson, Soil Mechanics Surface Sampler, Surveyor Program Results, NASA SP-184, 1969, pp. 171–179 1969.
[32] H.J. Moore, Estimates Of the Mechanical Properties of Lunar Surface Using Tracks and Secondary Impact Craters Produced by Blocks and Boulders (No. 70-229), US Dept. of the Interior, Geological Survey, 1970.
[33] N.C. Costes, W.D. Carrier III, J.K. Mitchell, R.F. Scott, Apollo 11: soil mechanics results, J. Soil Mech. Found. Div., Am. Soc. Civ. Eng. 96 (1970) 2045–2080.
[34] N.C. Costes, G.T. Cohron, D.C. Moss, Cone penetration resistance test-an approach to evaluating the in-place strength and packing characteristics of Lunar soils, Proc. 2nd Lunar Sci. Conf., 1971, 1971, pp. 1973–1987.
[35] J.K. Mitchell, L.G. Bromwell, W.D. Carrier III, N.C. Costes, R.F. Scott, Soil mechanics experiment, Apollo 14 Preliminary Sci. Rep., 1971, NASA SP_272, 1971, pp. 87–108.
[36] J.K. Mitchell, W.D. Carrier III, W.N. Houston, R.F. Scott, L.G. Bromwell, H.T. Durgunoglu, H.J. Hovland, D.D. Treadwell, N.C. Costes, Soil Mechanics, Apollo 16 Preliminary Science Report, NASA SP-315: 8 (1972), pp. 1–29.
[37] L.S. Gertsch, J. Rostamy, R. Gustafson, Review of Lunar regolith properties for design of low power Lunar excavators, Proc. International Conference on Case Histories in Geotechniqueal Engineering, 2008.
[38] S. Sture, A review of geotechniqueal properties of Lunar regolith simulants, Earth & Space 2006, ASCE, Houston, 2006, pp. 1–6. Tex, USA, 2006.
[39] H. Arslan, S. Sture, S. Batiste, Experimental simulation of tensile behavior of lunar soil simulant JSC-1, Mater. Sci. Eng. 478 (1–2) (2008) 201–207.
[40] H. Arslan, S. Batiste, S. Sture, Engineering properties of lunar soil simulant JSC-1A, J. Aero. Eng. 23 (1) (2010) 70–83.
[41] S.W. Perkins, S. Sture, H.-Y. Ko, Experimental, physical and numerical modelling of Lunar regolith and Lunar regolith structures, Proceedings of space III: Engineering, construction and operation in space I (1992) 189–200.
[42] D.S. McKay, J.L. Carter, W.W. Boles, C.C. Allen, J.H. Allton, JSC-1: a new Lunar soil simulant, Proc., Int. Symp. On Engineering, Construction, and Operations in Space IV, ASCE, Reston, VA, 1994, pp. 857–866.
[43] D.S. McKay, J.L. Carter, W.W. Boles, C.C. Allen, J.H. Alton, JSC-1: a new Lunar soil simulant in engineering, construction, and operations in space IV, in: R.G. Galloway, S. Lokajvol (Eds.), American Society of Civil Engineering, vol. 1, 1994, pp. 857–866 Reston, vol. A.
[44] J.L. Klosky, S. Sture, H.Y. Ko, F. Barnes, Mechanical properties of JSC-1 lunar regolith simulant, Engineering, Construction, and Operations in Space V, 1996, pp. 680–688.
[45] S.W. Perkins, C.R. Madson, Mechanical and load-settlement characteristics of two lunar soil simulants, J. Aero. Eng. 9 (1) (1996) 1–9.
[46] J.L. Klosky, S. Sture, H.-Y. Ko, F. Barnes, Geotechnical behavior of JSC-1 lunar regolith simulant, J of Aerospace Engineering, ASCE 13 (4) (2000) 680–688.
[47] H. Kanamori, S. Udagawa, T. Yoshida, S. Matsumoto, K. Takagi, Properties of lunar soil simulant manufactured in Japan, Space 98 (1998) 462–468.
[48] K.A. Alshibli, A. Hasan, Strength properties of JSC-1A lunar regolith simulant, Journal of Geotechniqueal and Geoenvironmental Engineering 135 (5) (2009) 673–679.
[49] X. Zeng, C. He, H. Oravec, A. Wilkinson, J. Agui, V. Asnani, Geotechniqueal properties of JSC-1A lunar soil simulant, J. Aero. Eng. 23 (2) (2010) 111–116.
[50] M. Jiang, L. Li, Y. Sun, Properties of TJ-1 lunar soil simulant, J. Aero. Eng. 25 (3) (2012) 463–469.
[51] C. He, X. Zeng, A. Wilkinson, Geotechniqueal properties of GRC-3 lunar simulant, J. Aero. Eng. 26 (3) (2013) 528–534.
[52] Z. Lu, L. Jianguo, Shear properties of lunar regolith simulants, Procedia Engineering 73 (2014) 178–185.
[53] E. Suescun-Florez, S. Roslyakov, M. Iskander, M. Baamer, Geotechniqueal properties of BP-1 lunar regolith simulant, J. Aero. Eng. 28 (5) (2015) 04014124.
[54] P.W. Weiblen, M.J. Murawa, K.J. Reid, Preparation of simulants for Lunar surface materials, Proc., Engineering Construction, and Operations in Space II, ASCE, Reston, VA, 1990, pp. 98–106.
[55] D.S. McKay, J.L. Carter, W.W. Boles, C.C. Allen, J.H. Allton, JSC-1: a new Lunar regolith simulant, Proc., 24th Lunar and Planetary Science Conf, Lunar and Planetary Institute, Houston, 1993, pp. 963–964.
[56] Y. Zheng, S. Wang, Z. Ouyang, Y. Zou, J. Liu, C. Li, J. Feng, CAS-1 Lunar soil simulant, Adv. Space Res. 43 (3) (2009) 448–454.
[57] D.B. Stoeser, D.L. Rickman, Preliminary Geological Findings on the BP-1 Simulant, (2010), p. 3 2010 https://www.nasa.gov/sites/default/files/atoms/files/nasa_tm_2010_216444.pdf.
[58] P. Delage, F. Karakostas, A. Dhemaied, M. Belmokhtar, P. Lognonné, M. Golombek, B. Banerdt, An investigation of the mechanical properties of some martian regolith simulants with respect to the surface properties at the InSight mission landing site, Space Sci. Rev. 211 (1–4) (2017) 191–213.
[59] H.J. Moore, R.E. Hutton, R.F. Scott, C.R. Spitzer, R.W. Shorthill, Surface materials of the Viking landing sites, J. Geophys. Res. 82 (28) (1977) 4497–4523.
[60] A. Shaw, R.E. Arvidson, R. Bonitz, J. Carsten, H.U. Keller, M.T. Lemmon, A. Trebi-Ollennu, Phoenix soil physical properties investigation, J. Geophys. Res. 114 (2009) E00E05.
[61] J. Bell, Martian polar processes, in: J. Bell (Ed.), The Martian Surface Composition, Mineralogy and Physical Properties, Cambridge Planet. Sci. Ser. vol. 9, Cambridge Univ. Press, 2008, pp. 578–598 chap. 25.
[62] L. Bell, Pneumatic membrane structures for space and terrestrial applications, Earth & Space 2008: Engineering, Science, Construction, and Operations in Challenging Environments, 2008, pp. 1–8.
[63] H.J. Moore, D.B. Bickler, J.A. Crisp, H.J. Eisen, J.A. Gensler, A.F.C. Haldemann, F. Pavlics, Soil-like deposits observed by Sojourner, the Pathfinder rover, J. Geophys. Res.: Plan 104 (E4) (1999) 8729–8746.
[64] K.E. Herkenhoff, M.P. Golombek, E.A. Guinness, J.B. Johnson, A. Kusack, L. Richter, R.J. Sullivan, S. Gorevan, In situ observations of the physical properties of the Martian surface, in: J.F. Bell III (Ed.), The Martian Surface: Composition, Mineralogy and Physical Properties, Cambridge University Press, Cambridge, 2008, pp. 451–467 2008. Chap. 20.
[65] R. Sullivan, R. Anderson, J. Biesiadecki, T. Bond, H. Stewart, Cohesions, friction angles, and other physical properties of Martian regolith from Mars Exploration Rover wheel trenches and wheel scuffs, J. Geophys. Res. 116 (E2) (2011).
[66] R.E. Arvidson, P. Bellutta, F. Calef, A.A. Fraeman, J.B. Garvin, O. Gasnault, R.C. Wiens, Terrain physical properties derived from orbital data and the first 360 sols of Mars Science Laboratory Curiosity rover observations in Gale Crater, J. Geophys. Res.: Plan 119 (6) (2014) 1322–1344.
[67] H.J. Moore, B.M. Jakosky, Viking landing sites, remote-sensing observations, and physical properties of Martian surface materials, Icarus 81 (1) (1989) 164–184.
[68] M. Golombek, M. Grott, G. Kargl, J. Andrade, J. Marshall, N. Warner, W.B. Banerdt, Geology and physical properties investigations by the InSight lander, Space Sci. Rev. 214 (5) (2018).
[69] H.J. Moore, G.D. Clow, R.E. Hutton, A summary of Viking sample-trench analyses for angles of internal friction and cohensions, J. Geophys. Res. 87 (1982) 10043–10050.

[70] H.J. Moore, R.E. Hutton, G.D. Clow, C.R. Spitzer, Physical Properties of the Surface Materials of the Viking Landing Sites on Mars, USGS Prof. Paper, 1987 1389, 222pp., 1987.
[71] P. Lognonné, W.B. Banerdt, D. Giardini, W.T. Pike, U. Christensen, P. Laudet, K.J. Hurst, SEIS: Insight's seismic experiment for internal structure of Mars, Space Sci. Rev. 215 (1) (2019) 12.
[72] P.H. Smith, L. Tamppari, R.E. Arvidson, D. Bass, D. Blaney, W. Boynton, E. DeJong, Introduction to special section on the phoenix mission: landing site characterization experiments, mission overviews, and expected science, J. Geophys. Res.: Plan 113 (E3) (2008).
[73] T. Spohn, M. Grott, S.E. Smrekar, et al., The heat flow and physical properties package (HP3) for the InSight mission, Space Sci. Rev. 214 (2018) 96, https://doi.org/10.1007/s11214-018-0531-4.
[74] T. Spohn, M. Grott, N. Müller, J. Knollenberg, C. Krause, T. Hudson, T. Wippermann, Mars regolith properties as constrained from HP3 mole operations and thermal measurements, EGU Gen. Assemb. (9163) (4-8 May 2020), https://doi.org/10.5194/egusphere-egu2020-9163.
[75] M. Golombek, N.H. Warner, J.A. Grant, et al., Geology of the InSight landing site on Mars, Nat. Commun. 11 (1) (2020), https://doi.org/10.1038/s41467-020-14679-1.
[76] H.A. Perko, J.D. Nelson, J.R. Green, Mars soil mechanical properties and suitability of mars soil simulants, J. Aero. Eng. 19 (3) (2006) 169–176.
[77] C.C. Allen, K.M. Jager, R.V. Morris, D.J. Lindstrom, M.M. Lindstrom, J.P. Lockwood, JSC MARS-1: a martian soil simulant, Space 98 (1998) 469–476.
[78] G.H. Peters, W. Abbey, G.H. Bearman, G.S. Mungas, J.A. Smith, R.C. Anderson, L.W. Beegle, Mojave Mars simulant—characterization of a new geologic Mars analog, Icarus 197 (2) (2008) 470–479.
[79] C. Brunskill, N. Patel, T.P. Gouache, G.P. Scott, C.M. Saaj, M. Matthews, L. Cui, Characterisation of Martian soil simulants for the ExoMars rover testbed, J. Terramechanics 48 (6) (2011) 419–438.
[80] X. Zeng, X. Li, S. Wang, S. Li, N. Spring, H. Tang, J. Feng, JMSS-1: a new Martian soil simulant, Earth Planets Space 67 (1) (2015).
[81] A. Banin, B.C. Clark, H. Wänke, H.H. Kieffer, et al. (Ed.), Surface Chemistry and Mineralogy, Mars, Univ. Arizona Press, Tucson, 1992, pp. 594–625.
[82] C.N. Foley, T.E. Economou, R.N. Clayton, W. Dietrich, Calibration of the Mars Pathfinder alpha proton X-ray spectrometer, J. Geophys. Res.: Plan 108 (E12) (2003).
[83] R. Rieder, R. Gellert, R.C. Anderson, J. Brückner, B.C. Clark, G. Dreibus, J. Zipfel, Chemistry of rocks and soils at meridiani planum from the alpha particle X-ray spectrometer, Science 306 (5702) (2004) 1746–1749.
[84] R. Gellert, Chemistry of Rocks and Soils in gusev Crater from the alpha particle X-ray spectrometer, Science 305 (5685) (2004) 829–832.
[85] K.M. Cannon, D.T. Britt, T.M. Smith, R.F. Fritsche, D. Batcheldor, Mars global simulant MGS-1: a Rocknest-based open standard for basaltic Martian regolith simulants, Icarus 317 (2019) 470–478.
[86] A.H. Stevens, E. Steer, A. McDonald, E.S. Amador, C.S. Cockell, Y-mars: an astrobiological analogue of martian mudstone, Earth and Space Science 5 (4) (2018) 163–174.
[87] J.L. Klosky, S. Sture, H.Y. Ko, F. Barnes, Helical anchors for combined anchoring and soil testing in lunar operations, Space 98 (1998) 489–494.
[88] M.M. Ettouney, H. Benaroya, Regolith mechanics, dynamics, and foundations, J. Aero. Eng. 5 (2) (1992) 214–229.
[89] N.I. Kömle, P. Weiss, K.L. Yung, Considerations on a suction drill for Lunar surface drilling and sampling: I. Feasibility study, Acta Geotechniquea 3 (3) (2008) 201–214.
[90] B.C. Chang, L.E. Bernold, T.S. Lee, Experimental study of lunar regolith anchoring forces, Earth and Space 2010: Engineering, Science, Construction, and Operations in Challenging Environments, 2010, pp. 1418–1422.
[91] T. Ebert, P. Larochelle, March). Simulation of soft regolith dynamic anchors for celestial exploration, 2016 IEEE Aerospace Conference, IEEE, 2016, pp. 1–7.
[92] P. Metzger, X. Li, C. Immer, J. Lane, ISRU implications for lunar and martian plume effects, 47th AIAA Aerospace Sciences Meeting Including the New Horizons Forum and Aerospace Exposition, 2009, p. 1204.
[93] J. Lee, B.C. Chang, S. Lee, T.S. Lee, Feasibility study on lunar concrete landing pad, Earth and Space 2012: Engineering, Science, Construction, and Operations in Challenging Environments, 2012, pp. 128–134.
[94] R.M. Kelso, R. Romo, C. Andersen, R.P. Mueller, T. Lippitt, N.J. Gelino, M. Hedlund, Planetary basalt field project: Construction of a lunar launch/landing pad, PISCES and NASA kennedy space center project update, Earth Space (2016) 653–667.
[95] P.J. Van Susante, P.T. Metzger, Design, test, and simulation of lunar and mars landing pad soil stabilization built with in situ rock utilization, Earth Space (2016) 642–652.
[96] P.J. Van Susante, K. Zacny, M. Hedlund, J. Atkinson, N. Gelino, R. Mueller, Robotic mars and lunar landing pad construction using in situ rocks, Earth Space (2018) 268–280.
[97] R.E. Ferguson, E. Shafirovich, J.G. Mantovani, Combustion joining of regolith tiles for in situ fabrication of launch/landing pads on the moon and mars, Earth Space (2018) 281–288.
[98] R. Romo, C. Andersen, K. Defore, K. Zacny, M. Thangavelu, T. Lippitt, Planetary lego: Designing a construction block from a regolith derived feedstock for in situ robotic manufacturing, Earth Space (2018) 289–296.
[99] N. Leach, A. Carlson, B. Khoshnevis, M. Thangavelu, Robotic construction by contour crafting: the case of lunar construction, Int. J. Architect. Comput. 10 (3) (2012) 423–438.
[100] N.R. Goins, A.M. Dainty, M.N. Toksöz, Lunar seismology: the internal structure of the Moon, J. Geophys. Res.: Solid Earth 86 (B6) (1981) 5061–5074.
[101] Y. Nakamura, G.V. Latham, H.J. Dorman, How we processed Apollo Lunar seismic data, Phys. Earth Planet. In. 21 (2–3) (1980) 218–224.
[102] R.C. Bulow, C.L. Johnson, P.M. Shearer, New events discovered in the Apollo lunar seismic data, J. Geophys. Res. 110 (2005) E10003.
[103] Y. Nakamura, G.V. Latham, H.J. Dorman, Apollo lunar seismic experiment-final summary, J. Geophys. Res. 87 (S01) (1982) A117.
[104] Y. Nakamura, J. Dorman, F. Duennebier, M. Ewing, D. Lammlein, G. Latham, High-frequency teleseismic events, Proc. Lunar Sci. Conf. 5th (1974) 2883–2890 1974.
[105] J. Oberst, Y. Nakamura, A seismic risk for the Lunar base, The Second Conf. On Lunar Bases and Space Activities of the 21st Century vol. 1, NASA, Washington, DC, 1992, pp. 231–233.
[106] D.R. Lammlein, Lunar seismicity and tectonics, Phys. Earth Planet. In. 14 (3) (1977) 224–273.
[107] N.R. Goulty, Tidal triggering of deep Moonquakes, Phys. Earth Planet. In. 19 (1) (1979) 52–58.
[108] N.R. Goins, A.M. Dainty, M.N. Toksöz, Seismic energy release of the Moon, J. Geophys. Res. 86 (B1) (1981) 378.
[109] J.C. Robinson, Statistically optimal stacking of seismic data, Geophysics 35 (3) (1970) 436–446.
[110] C. Frohlich, Y. Nakamura, The physical mechanisms of deep moonquakes and intermediate-depth earthquakes: how similar and how different? Phys. Earth Planet. In. 173 (3–4) (2009) 365–374.
[111] Y. Nakamura, G.V. Latham, H.J. Dorman, A.K. Ibrahim, J. Koyama, P. Horvath, Shallow Moonquakes: depth, distribution and implications as to the present state of the Lunar interior, Proc. Lunar Planet. Sci. Conf. loth (1979) 2299–2309 1979.
[112] F. Duennebier, G.H. Sutton, Thermal moonquakes, J. Geophys. Res. 79 (29) (1974) 4351–4363.
[113] F. Duennebier, Thermal movement of the regolith, Lunar and Planetary Science Conference Proceedings vol. 7, (1976, April), pp. 1073–1086.
[114] F. Duennebier, J. Dorman, D. Lammlein, G. Latham, Y. Nakamura, Meteoroid flux from passive seismic experiment data, Lunar and Planetary Science Conference Proceedings, vol. 6, 1975, pp. 2417–2426.
[115] F. Duennebier, G.H. Sutton, Meteoroid impacts recorded by the short-period component of Apollo 14 Lunar passive seismic station, J. Geophys. Res. 79 (1974) 4365–4374 1974a.
[116] F.K. Duennebier, Y. Nakamura, G.V. Latham, H.J. Dorman, Meteoroid storms detected on the moon, Science 192 (4243) (1976) 1000–1002.
[117] J. Dorman, S. Evans, Y. Nakamura, G. Latham, On the time-varying properties of the lunar seismic meteoroid population, Lunar and Planetary Science Conference Proceedings vol. 9, (1978), pp. 3615–3626.
[118] M.S. Robinson, S.M. Brylow, M. Tschimmel, D. Humm, S.J. Lawrence, P.C. Thomas, M.A. Caplinger, Lunar reconnaissance orbiter camera (LROC) instrument overview, Space Sci. Rev. 150 (1–4) (2010) 81–124.
[119] with, W.T. Pike, W. Banerdt, S. Smrekar, P. Lognonné, D. Giardini, D. Banfield, ... T. Spohn, Results from the Insight mission after a year and a half on mars, EGU General Assembly 22031 (2020) 4–8, https://doi.org/10.5194/egusphere-egu2020-22031 May.
[120] W.B. Banerdt, S.E. Smrekar, D. Banfield, et al., Initial results from the InSight mission on Mars, Nat. Geosci. (2020), https://doi.org/10.1038/s41561-020-0544-y.
[121] M. Knapmeyer, S.C. Stähler, M. van Driel, J.F. Clinton, W. Banerdt, M. Böse, R.C. Weber, Is there a seasonality of the martian seismic event rate? EGU General Assembly (4-8 May 2020), 2020.
[122] D. Giardini, P. Lognonné, W.B. Banerdt, et al., The seismicity of Mars, Nat. Geosci. (2020), https://doi.org/10.1038/s41561-020-0539-8.
[123] P. Lognonné, W.B. Banerdt, W.T. Pike, et al., Constraints on the shallow elastic and anelastic structure of Mars from InSight seismic data, Nat. Geosci. (2020), https://doi.org/10.1038/s41561-020-0536-y.
[124] A. Theinat, A. Modiriasari, A. Bobet, J. Melosh, S. Dyke, J. Ramirez, D. Gomez, Geometry and structural stability of lunar lava tubes, 2018 AIAA SPACE and Astronautics Forum and Exposition, 2018, p. 5185.
[125] A.K. Theinat, A. Modiriasari, A. Bobet, H.J. Melosh, S.J. Dyke, J. Ramirez, D. Gomez, Lunar lava tubes: morphology to structural stability, Icarus 338 (2020) 113442.
[126] M.M. Cohen, October). Selected precepts in lunar architecture, 34th COSPAR Scientific Assembly, 2002.
[127] B. Khoshnevis, A. Carlson, M. Thangavelu, ISRU-based Robotic Construction Technologies for Lunar and Martian Infrastructures, (2017).
[128] H. Benaroya, M. Nagurka, Space structures: issues in dynamics and control, a, J. Aero. Eng. 3 (4) (1990) 251–270.
[129] H. Benaroya, M. Ettouney, Framework for evaluation of lunar base structural concepts, J. Aero. Eng. 5 (2) (1992) 187–198.
[130] H. Benaroya, M. Ettouney, Design and construction considerations for lunar outpost, J. Aero. Eng. 5 (3) (1992) 261–273.
[131] M. Ettouney, H. Benaroya, N. Agassi, Cable structures and lunar environment, J. Aero. Eng. 5 (3) (1992) 297–310.
[132] H. Benaroya, Tensile-integrity structures for the moon, Appl. Mech. Rev. 46 (6) (1993) 326.
[133] S. Jolly, D. Happel, J. Sture, S., Design and construction of a shielded Lunar outpost, J. Aero. Eng. 4 (1994) 417–434.
[134] R.B. Malla, H.R. Adib-Jahromi, M.L. Accorsi, Simplified design method for braced double-skinned structure in lunar application, J. Aero. Eng. 8 (4) (1995) 189–195.
[135] H. Benaroya, Structures for manned habitation, Earth & Space 2006: Engineering, Construction, and Operations in Challenging Environment, 2006, pp. 1–8.

[136] F. Ruess, J. Schaenzlin, H. Benaroya, Structural design of a lunar habitat, J. Aero. Eng. 19 (3) (2006) 133–157.
[137] R.B. Malla, D. Chaudhuri, Analysis of a 3D frame—membrane structure for lunar base, Earth & Space 2006: Engineering, Construction, and Operations in Challenging Environment, 2006, pp. 1–8.
[138] C. Meyers, H. Toutanji, Analysis of lunar-habitat structure using waterless concrete and tension glass fibers, J. Aero. Eng. 20 (4) (2007) 220–226.
[139] R.B. Malla, D. Chaudhuri, Dynamic analysis of a 3-D frame-membrane lunar structure subjected to impact, Earth & Space 2008: Engineering, Science, Construction, and Operations in Challenging Environments, 2008, pp. 1–10.
[140] R.B. Malla, T.G. Gionet, Dynamic response of a pressurized frame-membrane lunar structure with regolith cover subjected to impact load, J. Aero. Eng. 26 (4) (2013) 855–873.
[141] E.J. Faierson, K.V. Logan, B.K. Stewart, M.P. Hunt, Demonstration of concept for fabrication of Lunar physical assets utilizing Lunar regolith simulant and a geo-thermite reaction, Acta Astronaut. 67 (1–2) (2010) 38–45.
[142] S. Mottaghi, H. Benaroya, Design of a lunar surface structure. II: seismic structural analysis, J. Aero. Eng. 28 (1) (2015) 04014053.
[143] S. Mottaghi, H. Benaroya, Design of a lunar surface structure. I: design configuration and thermal analysis, J. Aero. Eng. 28 (1) (2015) 04014052.
[144] J. Oberst, Unusually high stress drops associated with shallow moonquakes, J. Geophys. Res. 92 (B2) (1987) 1397–1405.
[145] E. Seedhouse, Bigelow expandable activity module, Bigelow Aerospace – Colonizing Space One Module at A Time, Springer International Publishing, 2015, pp. 87–98.
[146] D.A. Litteken, March). Inflatable technology: using flexible materials to make large structures, Society of Photo-Optical Instrumentation Engineers (SPIE) Conference Series vol. 10966, (2019).
[147] P.S. Nowak, W.Z. Sadeh, L.A. Morroni, Geometric modeling of inflatable structures for lunar base, J. Aero. Eng. 5 (3) (1992) 311–322.
[148] M.D. Vanderbilt, M.E. Criswell, W.Z. Sadeh, Structures for a Lunar Base, SPACE 88 Engineering, Construction, and Operations in Space, Proceedings of the ASCE, New York, 1988, pp. 352–361.
[149] W. Sadeh, M. Criswell, Inflatable Structures for a Lunar Base, Space Programs and Technologies Conference and Exhibit, 1993.
[150] J.E. Abarbanel, T.A. Bateman, M.E. Criswell, W.Z. Sadeh, A framing system for a lunar/martian inflatable structure, Engineering, Construction, and Operations in Space V (1996) 1069–1075.
[151] D. Cadogan, J. Stein, M. Grahne, Inflatable composite habitat structures for Lunar and mars exploration, Acta Astronaut. 44 (7–12) (1999) 399–406.
[152] K.J. Kennedy, ISS TransHab: Architecture Description, SAE Technical Paper, 1999 No. 1999-01-2143.
[153] T.A. Bateman, J.E. Abarbanel, M.E. Criswell, Structural modifications to the framing system of a proposed lunar/Martian inflatable structure, Space (2000) 424–430 2000.
[154] P. Harris, K. Kennedy, Wound construction of inflatable space structures, Space (2000) 417–423 2000.
[155] C.H. Jenkins, M. Tampi, Local membrane vibrations and inflatable space structures, Space (2000) 410–416 2000.
[156] A. Borin, M. Fiscelli, An inflatable living concept, Engineering, Construction, and Operations in Challenging Environments: Earth and Space 2004, 2004, pp. 797–804.
[157] M.E. Criswell, J.S. Carlson, Concepts for the design and construction of a modular inflatable habitat, Engineering, Construction, and Operations in Challenging Environments: Earth and Space 2004, 2004, pp. 9–16.
[158] C.M. Adams, G. Petrov, The surface endoskeletal inflatable module (SEIM), Earth & Space 2006: Engineering, Construction, and Operations in Challenging Environment, 2006, pp. 1–8.
[159] C. Brandt-Olsen, A. Coward, D. Horswill, Mars Science City–Designing a future habitat in space, Proceedings of IASS Annual Symposia, vol. 2018, International Association for Shell and Spatial Structures (IASS), 2018, July, pp. 1–8 No. 1.
[160] A.G. Cherniavsky, V.I. Gulyayev, V.V. Gaidaichuk, A.I. Fedoseev, New developments in large deployable space antennae at SPA EGS, Engineering, Construction, and Operations in Challenging Environments: Earth and Space 2004, 2004, pp. 954–959.
[161] E. Medzmariashvili, S. Tserodze, N. Tsignadze, M. Sanikidze, L. Datashvili, A. Sarchimelia, G. Bedukadze, A new design variant of the large deployable space reflector, Earth & Space 2006: Engineering, Construction, and Operations in Challenging Environment, 2006, pp. 1–8.
[162] T.T. Ng, Numerical simulations of a deployable structure, Earth & Space 2006: Engineering, Construction, and Operations in Challenging Environment, 2006, pp. 1–6.
[163] M. Tinker, P.V. Hull, M.P. SanSoucie, A. Roldan, Inflatable and deployable structures for surface habitat concepts utilizing in-situ resources, Earth & Space 2006: Engineering, Construction, and Operations in Challenging Environment, 2006, pp. 1–8.
[164] S.R. Woodruff, E.T. Filipov, Advanced materials and designs for hydraulic, earth, and aerospace structures, Earth Space (2018) 824–832.
[165] M.C. Roman, E.A. Eberly, R.P. Mueller, S. Deutsch, NASA centennial challenge: Three dimensional (3D) printed habitat, Earth Space (2016) 333–342.
[166] B.J. Pletka, Processing of Lunar Basalt Materials. Resources of Near Earth Space, University of Arizona Press, 1993, pp. 325–350.
[167] R.P. Mueller, S. Howe, D. Kochmann, H. Ali, C. Andersen, H. Burgoyne, W. Chambers, A. Zelhofer, Automated additive construction (AAC) for earth and space using in situ resources, Earth and Space 2016: Engineering for Extreme Environments - Proceedings of the 15th Biennial International Conference on Engineering, Science, Construction, and Operations in Challenging Environments, 2016, pp. 354–377.
[168] V.K. Balla, L.B. Roberson, G.W. O'Connor, S. Trigwell, S. Bose, A. Bandyopadhyay, First demonstration on direct laser fabrication of Lunar regolith parts, Rapid Prototyp. J. 18 (6) (2012) 451–457.
[169] A. Goulas, J.G.P. Binner, R.A. Harris, R.J. Friel, Assessing extraterrestrial regolith material simulants for in-situ resource utilisation based 3D printing, Applied Materials Today 6 (2017) 54–61.
[170] A. Goulas, J.G. Binner, D.S. Engstrøm, R.A. Harris, R.J. Friel, Mechanical behaviour of additively manufactured Lunar regolith simulant components, Proc. IME J. Mater. Des. Appl. 233 (8) (2018) 1629–1644.
[171] S. Lim, V.L. Prabhu, M. Anand, L.A. Taylor, Extra-terrestrial construction processes – advancements, opportunities and challenges, Adv. Space Res. 60 (7) (2017) 1413–1429.
[172] M. Magoffin, J. Garvey, Lunar glass production using concentrated solar energy, Space Programs and Technologies Conference, 1990, p. 3752.
[173] T.D. Lin, S.B. Skaar, J.J. O'Gallagher, Proposed remote-control, solar-powered concrete production experiment on the moon, J. Aerospace Eng. 10 (2) (1997) 104–109.
[174] P. Hintze, J. Curran, T. Back, Lunar surface stabilization via sintering or the use of heat cured polymers, 47th AIAA Aerospace Sciences Meeting Including the New Horizons Forum and Aerospace Exposition, 2009, p. 1015.
[175] A. Meurisse, A. Cowley, S. Cristoforetti, A. Makaya, L. Pambaguian, M. Sperl, Solar 3D printing of lunar regolith, European Lunar Symposium 2016, Amsterdam, the Netherlands, 2016.
[176] S. Allan, B. Merritt, B. Griffin, P. Hintze, H. Shulman, High temperature microwave dielectric properties and processing of JSC-1AC Lunar simulant, J. Aerospace Eng. 26 (4) (2013) 874–881.
[177] P.E. Hintze, S. Quintana, Building a Lunar or martian launch pad with in situ materials: recent laboratory and field studies, J. Aerospace Eng. 26 (1) (2013) 134–142.
[178] S. Allan, J. Braunstein, I. Baranova, N. Vandervoort, M. Fall, H. Shulman, Computational modeling and experimental microwave processing of JSC-1A Lunar simulant, J. Aerospace Eng. 26 (1) (2013) 143–151.
[179] L.A. Taylor, T.T. Meek, Microwave sintering of Lunar soil: properties, theory, and practice, J. Aerospace Eng. 18 (3) (2005) 188–196.
[180] L.A. Taylor, C. Pieters, A. Patchen, D.-H.S. Taylor, R.V. Morris, L.P. Keller, D.S. McKay, Mineralogical and chemical characterization of Lunar highland soils: insights into the space weathering of soils on airless bodies, J. Geophys. Res.: Plan 115 (E2) (2010).
[181] B. Khoshnevis, J. Zhang, Extraterrestrial construction using contour crafting, 23rd Annual International Solid Freeform Fabrication Symposium - an Additive Manufacturing Conference, SFF 2012, 2012, pp. 250–259.
[182] M. Barmatz, D. Steinfeld, M. Anderson, D. Winterhalter, March). 3D microwave print head approach for processing lunar and mars regolith, Lunar and Planetary Science Conference vol. 45, (2014), p. 1137.
[183] S. Lim, M. Anand, Space architecture for exploration and settlement on other planetary bodies – in-Situ Resource Utilisation (ISRU) based structures on the Moon, European Lunar Symposium (ELS2014), London, 15–16 May, 2014.
[184] V. Srivastava, S. Lim, M. Anand, Microwave processing of Lunar soil for supporting longer-term surface exploration on the Moon. Special Issues, Space Pol. J 37 (2) (2016) 92–96.
[185] G. Cesaretti, E. Dini, X. De Kestelier, V. Colla, L. Pambaguian, Building components for an outpost on the Lunar soil by means of a novel 3D printing technology, Acta Astronaut. 93 (2013) 430–450.
[186] M. Thangavelu, Critical Strategies for Return to the moon: altair dust Mitigation and real-time teleoperations concepts, Joint Annual Meeting of LEAG-ICEUM-SRR, vol. 4056, 2008, October.
[187] M. Thangavelu, MALEO: modular Assembly in low earth orbit: alternate Strategy for lunar base development, J. Aero. Eng. 4 (3) (1991) 256–273.
[188] L. Bell, G. Trotti, J. Brown, N. Bhattacharya, N. Moore, T. Polette, L. Toups, Manned Lunar Outpost. Design Considerations for Three Key Elements in an Initial Manned Lunar Outpost, (1988).
[189] L. Bell, G. Trotti, Earth-based analogs of lunar and planetary facilities, Lunar Bases and Space Activities of the 21st Century, 1992, September.
[190] X. De Kestelier, E. Dini, G. Cesaretti, V. Colla, L. Pambaguian, Lunar Outpost Design. Research and Development, (2015) Available online at: https://www.fosterandpartners.com/media/2634652/Lunar_outpost_design_foster_and_partners.pdf.
[191] S. Wilkinson, J. Musil, J. Dierckx, I. Gallou, X. De Kestelier, Autonomous additive construction on mars. Earth and space 2016: engineering for extreme environments, Proceedings of the 15th Biennial International Conference on Engineering, Science, Construction, and Operations in Challenging Environments, 2016, pp. 343–353.